Identification of cyclic-di-GMP-modulating protein residues by bi-directionally evolving a social trait in *Pseudomonas fluorescens*

Collin Kessler[1] and Wook Kim[1*]

[1] Department of Biological Sciences, Duquesne University, Pittsburgh, Pennsylvania, United States of America

* Corresponding author

Email: kimw1@duq.edu

Abstract

Modulation of the intracellular cyclic di-guanosine monophosphate (c-di-GMP) pool is central to the formation of structured bacterial communities. Genome annotations predict the presence of dozens of conserved c-di-GMP catalytic enzymes in many bacterial species, but the functionality and regulatory control of the vast majority remain underexplored. Here, we begin to fill this gap by utilizing an experimental evolution system in *Pseudomonas fluorescens* Pf0-1, which repeatedly produces a unique social trait through bidirectional transitions between two distinct phenotypes converging on c-di-GMP modulation. Parallel evolution of 33 lineages captured 147 unique mutations among 191 evolved isolates in genes that are empirically demonstrated, bioinformatically predicted, or previously unknown to impact the intracellular pool of c-di-GMP. Quantitative chemistry confirmed that each mutation causing the phenotypic shift predictably amplifies or reduces c-di-GMP production. We integrate our mutation, phenotype, and quantification data with current models of known regulatory and catalytic systems, describe a previously unknown relationship between a regulatory component of branched-chain amino acid biosynthesis and c-di-GMP production, and predict functions of unexpected proteins that clearly impact c-di-GMP production. Sequential mutations that continuously disrupt or recover c-di-GMP production across discrete functional elements suggest a complex and underappreciated interconnectivity within the c-di-GMP regulome of *P. fluorescens*.

Author summary

Microbial communities comprise densely packed cells where competition for space and resources is fierce. Simply by growing a colony of bacterial cells in the laboratory, one could reliably observe mutant genotypes that solve the problem of overcrowding. For example, mutant cells with a dry (D) phenotype are always selected from a population with a mucoid (M) phenotype, and vice versa, because M and D cells physically work together to spread away from the overcrowded colony. D cells

44 produce high levels of c-di-GMP and M cells produce low levels, so each mutation that causes the
45 phenotypic shift impacts c-di-GMP production. C-di-GMP is an intracellular signaling molecule that
46 regulates diverse phenotypes, which provide benefit to bacteria, but cause tremendous clinical and
47 environmental problems. Why many bacteria possess dozens of enzymes that are known or predicted to
48 produce c-di-GMP is a major question in the field. Here, we take advantage of the bi-directional
49 selection of M and D phenotypes to identify key residues that could force these enzymes to turn on or
50 off. Several unexpected proteins were also identified, but very little is known about them. Our extensive
51 dataset should stimulate functional studies of many commonly shared and understudied proteins that
52 modulate c-di-GMP.
53
54 **Introduction**
55 Microbes utilize diverse signaling mechanisms to adapt and respond to a dynamic environment.
56 Cyclic di-guanosine monophosphate (c-di-GMP) is a ubiquitous secondary messenger in bacteria and
57 high intracellular levels of c-di-GMP characteristically repress flagellar motility while stimulating the
58 expression of biofilm-formation genes [1–4]. Numerous c-di-GMP binding proteins and riboswitches
59 respond to intracellular levels of c-di-GMP to also regulate cellular morphology, virulence factors,
60 antibiotic production, and the cell cycle [5,6]. C-di-GMP is synthesized from two molecules of GTP by a
61 diguanylate cyclase (DGC) and hydrolyzed by a phosphodiesterase (PDE) [1]. DGCs and PDEs are
62 identified by the GGDEF or EAL/HD-GYP domains, respectively, and there are also hybrid proteins with
63 both DGC and PDE functions [7,8]. *Pseudomonas* spp. typically possess greater than 50 predicted DGCs
64 or PDEs [9]. Specific signaling pathways or regulators have been characterized to independently regulate
65 several DGCs and PDEs [10–17], and some have been demonstrated to be under allosteric control,
66 where a certain range of c-di-GMP levels either initiate or prevent enzymatic activity [18–22]. However,

67 the function of the vast majority of bioinformatically predicted DGCs and PDEs have not been
68 empirically validated and their regulatory mechanisms remain unknown [23].
69 A previous experimental evolution study described the bidirectional evolution of mucoid (M)
70 and dry (D) colony phenotypes in *P. fluorescens* Pf0-1, which likely occurs through c-di-GMP oscillation
71 [24]. An aging colony of M cells repeatedly produces spreading fans at the perimeter, which comprise
72 the original M cells along with new D mutant cells that produce a dry and wrinkly colony morphology on
73 their own. Additionally, an aging colony of D cells also repeatedly generates spreading fans, which
74 comprise the original D cells along with a new mutant that appears phenotypically identical to the
75 ancestral M. This bidirectional selection of M and D phenotypes occurs continuously because M and D
76 cells self-organize in space and physically work together to spread out from the nutrient-poor and
77 crowded conditions of dense colony growth, and neither type is capable of spreading out on their own.
78 Genetic analyses of five evolved isolates revealed characteristic mutations in *wsp* genes to suggest that
79 c-di-GMP production is likely elevated in D and reduced in M [24].
80 Here, we carry out a large-scale parallel evolution experiment using the bidirectional M-D
81 system to identify 147 unique genes that are empirically demonstrated, bioinformatically predicted, or
82 previously unknown to impact c-di-GMP levels. We expand the current model of c-di-GMP production by
83 the Wsp signal transduction system and identify unique missense mutations outside the conserved
84 catalytic domain of numerous DGCs that stimulate enzymatic activity. We also describe proteins with no
85 previous associations to c-di-GMP production that appear to influence the activity of several DGCs,
86 including a regulatory component of the branched-chain amino acid (BCAA) biosynthesis pathway.
87 Lastly, we map the interconnectivity of the c-di-GMP regulome through sequential mutations that
88 disrupt or recover c-di-GMP production across functionally discrete systems.
89
90

Results and Discussion

Bidirectional evolution of mucoid and dry phenotypes occurs through intracellular c-di-GMP pool oscillation

The bidirectional selection of mucoid (M) and dry (D) phenotypes occurs continuously in our experimental system [24] because neither type is capable of spreading out on their own, but a colony of initially mixed M and D cells readily spreads out in a radial pattern without requiring additional mutations (Fig. 1A). With the expectation that a large-scale utilization of this experimental evolution system could identify diverse mechanisms of c-di-GMP modulation, we initially set up 25 parallelly evolving lineages of M. As anticipated, we observed bidirectional transitions between M and D phenotypes across all lineages. In total, we isolated over 600 strains, analyzed genome sequences of 191 strains, and quantified c-di-GMP in a subset of 56 strains. Remarkably, we detected a single mutation associated with each phenotypic transition, with the exception of only few additional silent mutations across all genome sequences (Fig. S1, Table S1, Table S1 – Source Data 1). Genome sequencing successive strains within each lineage provided an internal control, which confirmed the exclusive presence of the respective preceding mutations. Among the 147 unique mutations detected, 81 mutations were in *wsp* genes and 66 mutations were in other genes including those that are hypothetical. Motility assays showed that all D strains were non-motile and all M strains were motile as expected, and LC-MS/MS quantification confirmed that c-di-GMP was elevated in all D strains relative to their respective parent M strain (Table S1). For the sake of an accessible narrative, we will primarily refer to five simplified lineages (Fig. 1B), with corresponding c-di-GMP measurements (Fig. 1C) and colony morphologies (Fig. S2).

The combination of our mutation, phenotype, and c-di-GMP quantification data could serve as a powerful resource for deducing protein and pathway functions. Furthermore, successive patterns of mutations across generations of independently evolving lineages could reveal previously unknown

115 connectivity between discrete regulatory and catalytic elements. Notably, many mutations that disrupt
116 or recover c-di-GMP production sequentially flank specific mutations in the Wsp signaling system, the
117 most extensively studied c-di-GMP regulatory system in *Pseudomonas* spp. [17]. We first focus on
118 sequential mutations in the Wsp system to reveal both predictable and surprising evolutionary
119 innovations to modulate c-di-GMP production. Several missense mutations observed in Wsp proteins
120 identified in this study overlap with comparable mutations from various *Pseudomonas* and *Burkholderia*
121 studies that we had previously compiled from the literature [17] (Fig. 2). However, the vast majority of
122 our mutations had never been observed and many occur outside functionally annotated domains. The
123 data presented in Fig. 2 represent the most comprehensive record of functionally important residues of
124 the Wsp system to date and empower our predictions of mutation consequences.
125

126 **Diverse mutations converge on the Wsp signal transduction system that dynamically rewire signal**
127 **flow to produce a spectrum of functional states**

128 The Wsp signal transduction system was first reported two decades ago in *P. fluorescens* [25]
129 and continues to serve as the primary model system of c-di-GMP regulation in pseudomonads. The Wsp
130 system comprises seven proteins encoded in a monocistronic operon under the control of an
131 unidentified transcriptional regulator [26], and the current functional model is based on a combination
132 of empirical studies and predictions based on homologies to the chemotaxis system in *Escherichia coli*
133 [17]. The main differences with the latter are that the signal cascade is initiated by the extracellular
134 sensory domain of WspA detecting surface contact [27,28] to ultimately drive c-di-GMP production by
135 the DGC WspR (Fig. 3).

136 Given that a mutation in any one of the seven Wsp protein coding genes could potentially
137 increase or decrease c-di-GMP production through WspR, we expected *wsp* genes to be a common
138 target in our parallel evolution experiments. Indeed, the vast majority of the first transitions from the

139 ancestral M to D occurred through a *wsp* mutation and we generally observed mutations in other genes
140 to follow once the Wsp system became functionally crippled (Table S1). Such a striking pattern suggests
141 that the Wsp system has the greatest capacity to contribute to the overall intracellular pool of c-di-GMP
142 under our experimental conditions. Indeed, high c-di-GMP production is mostly associated with *wsp*
143 mutations (Table S1). We thus set up an independent lineage to commence with an engineered *ΔwspC*
144 M strain (Fig. 4, strain 1.0), under the expectation that the deletion of *wspC* would prevent further
145 mutations within the Wsp system, since the removal of the methyltransferase should prevent WspA
146 signaling (Fig. 3). However, we detected a missense mutation in WspA (A381V) within the signaling
147 domain [17] in the first D progeny strain 1.1. We had previously described the same A381V mutation in
148 an independently evolved D strain with an unaltered *wspC* gene, which is predicted to lock WspA in a
149 constitutively active conformation to stimulate WspE even in the absence of methylation by WspC [24].
150 The subsequent M progeny strain 1.2 carries a missense mutation in in WspB (L136P), which likely
151 disrupts the interaction between WspA and WspE to terminate c-di-GMP production. We next observed
152 an in-frame deletion of amino acid residues 674-696 spanning the phosphoreceiver domain of WspE in
153 the D progeny strain 1.3. The restoration of c-di-GMP production in this strain suggests that the
154 observed deletion forces WspE to conform an activated state without being stimulated by WspA.
155 Accordingly, mutations within the conserved phosphoreceiver domain of CheY, a WspE homolog in
156 *Escherichia coli*, can activate the protein without phosphorylation [29,30]. In addition, the DGC activity
157 of WspR in *P. aeruginosa* could be modulated in a phosphorylation-independent manner [16,31]. The
158 subsequent M progeny strain 1.4 carries a frameshift mutation in *wspE*, which should terminally shut
159 down the Wsp system, and the c-di-GMP level was reduced as predicted. C-di-GMP production was
160 restored in this lineage once again in the following D strain 1.5 through a missense mutation in DgcH
161 (V459G), a bioinformatically predicted DGC in *P. aeruginosa* PAO1 that impacts biofilm formation [32].
162 While DgcH shares a namesake with the DGCs DgcA, DgcB, and DgcC, no known interactions exist

163 between these proteins and DgcH. DgcH is not only capable of producing c-di-GMP, but at one of the
164 highest levels detected in our study (Fig. 4, Table S1). In contrast to the Wsp system, it is difficult to
165 predict functional consequences of mutations in other DGCs, since so little is known beyond their
166 conserved catalytic domain.

167 Lineages 2-5 were commenced with the ancestral M strain with the native Wsp system intact
168 (Fig. 4). Much like in lineage 1, initial mutations appear to artificially activate the Wsp system that are
169 followed by surprisingly similar patterns of sequential mutations in various *wsp* genes to oscillate c-di-
170 GMP production. Lineages 2 and 3 began with the first respective D strain possessing a unique in-frame
171 deletion that partially spans the predicted methylation helices of WspA. Lineage 5 began with a
172 missense mutation in the phosphoreceiver domain of WspF (P105S), which likely disrupts its methyl-
173 esterase activity to keep WspA in an activated state (Fig. 3, Fig. 4). This activation is undone in the
174 following M strain by an in-frame deletion in *wspA* that removes the amino acid residue S329, then c-di-
175 GMP production is restored again in the next D strain through an in-frame deletion of residues 282-296
176 in WspA. This deletion falls within the same deleted region as those observed in lineages 2 and 3 (Fig. 4).
177 Although methylation of WspA remains to be empirically demonstrated, its predicted methylation
178 helices clearly have a functional role in Wsp signaling as they were commonly mutated to activate c-di-
179 GMP production (Fig. 2). Based on our mutation data and homologies to Tsr-methylation in the
180 chemotaxis system of *E. coli* [33], we predict that the following two sets of residues are methylated in
181 WspA: Q285, E292, E299 and Q502, E512. The linker region of WspA that connects the HAMP and
182 signaling domains contains the first set of E and Q residues, which undergo methyl esterification in Tsr
183 during chemotaxis. A second linker region between the signaling domain and predicted WspC-WspF
184 docking site contains the second set of E and Q residues (Fig. 2). The addition of a bulky methyl group to
185 the Tsr methylation site of the coiled-coil domain alters the topology of the alpha helix which is relayed
186 through the linker domain and into the signaling domain [34]. WspA is expected to undergo a similar

187 conformational change upon methylation and our data suggest that the deletion of the putative
188 methylation sites mimics a methylated state, which is relayed through its linker domain and into the
189 signaling domain that interacts with WspB, WspD, and WspE. Furthermore, missense mutations in
190 WspA's signaling domain (A381V in lineage 1, V380A in lineage 4, and several others as shown in Fig. 2)
191 independently stimulate c-di-GMP production, which likely bypass the methylation requirement to
192 activate WspE.

193 Mutations that artificially stimulate WspA were typically followed by a missense mutation in
194 WspB, WspD, or WspE (Table S1). A missense mutation in WspD (W90L) in lineage 2 reduced c-di-GMP
195 production like the WspB (L136P) mutation in lineage 1 (Fig. 4). The functional roles of WspB and WspD
196 in signal relay are loosely modeled after homology to CheW of *E. coli*, which remains as the least
197 characterized protein in the chemotaxis system. Mutations in CheW that successfully disrupt signal
198 transduction are largely limited to five unique amino acid clusters that situate on the protein surface
199 and are essential for the docking of CheW to Tsr [35]. WspB and WspD also possess six and seven highly
200 conserved amino acid clusters, respectively [17]. Our WspB L135P and WspD W90L mutations fall within
201 these conserved clusters that likely situate on the surface of WspB and WspD and natively act as docking
202 sites for WspA and WspE to permit signal relay. We also observed additional missense and in-frame
203 deletion mutations in WspB and WspD that independently impact c-di-GMP production (Fig.2, Table S1),
204 confirming that that both WspB and WspD are necessary for Wsp signal transduction through domains
205 and interactions that remain to be characterized. Following the WspD (W90L) mutation in lineage 2, the
206 subsequent D strain 2.3 then restores c-di-GMP production through the missense mutation in
207 Pfl01_3147 (A383S) (Fig. 4), which is annotated as a hypothetical protein, but we found homology to an
208 N-ethylammeline chlorohydrolase. We will thus refer to this protein as NarA (N-ethylammeline
209 chlorohydrolase associated c-di-GMP regulator). Surprisingly, we observed a shift back to the M
210 phenotype in strain 2.4 through a nonsense mutation in *wspD* (Table S1, Fig. S1), which suggests that the

211 *narA* mutation in strain 2.3 enhances c-di-GMP production by functionally complementing the preceding
212 WspD W90L mutation in strain 2.2.

213 Loss-of-function mutations (i.e. nonsense and frameshift mutations) in *wspE* were exclusively
214 associated with D to M transitions throughout all lineages to reduce c-di-GMP production (Table S1).
215 These observations are not particularly surprising, since WspR cannot be phosphorylated in the absence
216 of a functional WspE (Fig. 3). However, we also observed an interesting sequence of mutations that
217 oscillate c-di-GMP production through multiple missense mutations in WspE. In lineage 4, a missense
218 mutation in the HATPase domain of WspE (D390N), likely impacting the kinase activity in a negative
219 manner, caused a shift to the M phenotype. Surprisingly, the subsequent D strain 4.5 recovered c-di-
220 GMP production through an in-frame deletion of the methylation helices of WspA. Although we
221 observed the same in-frame deletion in the D strain 2.1 as the first transitional step in lineage 2, the
222 relative increase in c-di-GMP production was much smaller in strain 4.5 (Fig. 4). These results are
223 consistent with WspE (D390N) retaining residual function in signal relay. WspE appears to be further
224 disabled by another missense mutation V441A in the M strain 4.6, which again affects the HATPase
225 domain to decrease c-di-GMP production. Incredibly, the following D strain 4.7 strongly recovers c-di-
226 GMP production through the missense mutation S472C in the same HATPase domain of WspE, which
227 replaces the polar amino acid serine with the non-polar amino acid cysteine. Non-polar amino acids are
228 important in protein-ATP binding [36], and this mutation appears to allow WspE to interact with ATP
229 more efficiently in the presence of debilitating mutations. In contrast, as observed in lineage 1, multiple
230 missense and in-frame deletions were observed in the phosphoreceiver domain of WspE to exclusively
231 stimulate c-di-GMP production (Fig. 2). In particular, the D648G mutation observed in this study was
232 also previously identified in an independently evolved D strain and predicted to artificially trigger an
233 activated conformation in a phosphorylation-independent manner [24]. Such mutations decouple WspE
234 from WspA-induced activation, and were often the evolutionary solution to recover c-di-GMP

235 production when the upstream signaling components of the Wsp system became functionally crippled
236 (Table S1).
237
238 **Many DGCs are functionally capable of causing the M to D shift independently from WspR**
239 Sequential patterns of mutations and c-di-GMP quantification across all 33 lineages indicate that
240 the DGC DgcH is also a dominant contributor to the intracellular c-di-GMP pool under our experimental
241 conditions (Table S1). Other known or predicted DGCs were typically targeted to modulate c-di-GMP
242 levels after the Wsp system and DgcH became genetically dysfunctional. One other exception may be
243 MorA, which represents the first mutation target in two lineages (Table S1). The first D strain 4.1 of
244 lineage 4 carries an in-frame deletion mutation in *dgcH* that removes amino acid residues 524-537 (Fig.
245 4, Fig. 5). Interestingly, the GGDEF diguanylate cyclase domain of DgcH spans residues 537-693. The
246 observed in-frame deletion adjacent to this domain appears to activate c-di-GMP production, though we
247 cannot currently speculate on the mechanism due to limited understanding of DgcH. We observed a
248 reduction in c-di-GMP in the following M strain 4.2, which has a missense mutation in DgcH (L634P). A
249 search against NCBI's conserved domain database identifies that the residues 619-643 contain the
250 inhibitory I-site [22,37], with residue N637 as the predicted interaction site with c-di-GMP. Our mutation
251 data supports this annotation and the likelihood that DgcH is under allosteric control by c-di-GMP. We
252 also detected the I-site in other DGCs, with MorA being the lone exception, but no associated mutations
253 were found (Fig. 5). The L634P mutation in DgcH could mimic a c-di-GMP bound state to cause the
254 observed reduction in c-di-GMP. We cannot discount the possibility of additional regulatory
255 mechanisms, since we observe other missense and in-frame deletion mutations across the coding
256 sequence of DgcH (Fig. 5). As already discussed above, the V459G mutation greatly increased c-di-GMP
257 production in lineage 1 (Fig. 4), and in lineage 27, the Q454P mutation caused a shift to the D phenotype
258 then reverted back to the M phenotype through another missense mutation (Q148P) (Table S1). In

259 addition to DgcH, missense mutations in other DGCs caused bi-directional shifts. However, most
260 activating mutations were found outside their conserved catalytic domain (Fig. 5). To the best of our
261 knowledge, no specific functional studies have been carried out to characterize the other
262 bioinformatically predicted domains. Nevertheless, we have clearly established that these mutations
263 impact c-di-GMP production, which should stimulate future studies to characterize their catalytic and/or
264 regulatory consequences.
265
266 **Mutations in genes with previously unknown associations with c-di-GMP production integrate with**
267 **Wsp or other DGC mutations to modulate c-di-GMP levels**
268 We also observed mutations in bioinformatically annotated genes with no known associations
269 to c-di-GMP modulation, but with clear associations with Wsp components and other DGCs. This pattern
270 is best represented in lineage 5 (Fig. 4). Like most lineages, mutations initially accumulate within *wsp*
271 genes and deregulate the Wsp system. Subsequent strains D 5.5 and M 5.6 carry mutations that activate
272 then deactivate the DGC SadC, respectively. The activating mutation occurs in the 5'UTR of *sadC* and
273 likely increases the expression of the DGC as evidenced by increased intracellular c-di-GMP. This
274 activation is then undone through an in-frame deletion of the L25 residue in SadC. Surprisingly, strain
275 5.7 returns this lineage to the D phenotype through a missense mutation in IlvH (G150S), which is
276 predicted to function in the biosynthesis of branched chain amino acids (BCAA). We observed three
277 independent missense mutations in IlvH across our study that exclusively cause a phenotypic shift from
278 M to D and reduced motility (Table S1). Accordingly, quantification of c-di-GMP shows that each of these
279 three mutations significantly increases c-di-GMP respective to their immediate M parent (Fig. 6). These
280 results indicate that a previously unknown relationship between BCAA biosynthesis and c-di-GMP
281 production may exist, and we explore this relationship in detail below.

282 Lineage 5 returns to the M phenotype in strain 5.8 through a missense mutation in the
283 hypothetical protein Pfl01_0730 (D115N) (Fig. 4). This protein, hereon ParA (PAP2 associated c-di-GMP
284 regulator), shares homology with the PAP2 superfamily of proteins, suggesting that it may be involved in
285 phospholipid turnover and impact the bioavailability of phosphate within the cell [38]. Although we
286 found the relative decrease in c-di-GMP in strain 5.8 to be not statistically significant from its parent
287 likely due to technical noise (Fig. 6), the observed mutation clearly drives the phenotypic transition from
288 D to M. Furthermore, if this mutation does not impact c-di-GMP levels, then we would not expect a
289 further transition through elevated c-di-GMP production. Indeed, we captured two independent
290 transitions back to the D phenotype, both with substantially increased c-di-GMP levels (Fig. 4). Strains
291 5.9a and 5.9b are sister strains that have developed unique chimeric Wsp proteins. Both chimeric
292 proteins (WspA::D and WspB::D) contain identical partial segments of WspD commencing at residue
293 158, situated immediately adjacent to the in-frame deletion detected in their common ancestral strain
294 5.4, which previously deactivated the Wsp system (Fig. 4). To determine whether or not these chimeric
295 proteins alone are sufficient to drive the phenotypic shift from M to D, we replaced the corresponding
296 native Wsp proteins in the ancestral M strain with each chimeric protein. In parallel, we also replaced
297 the corresponding naturally modified Wsp proteins in the immediate parental M strain 5.8 with each
298 chimeric protein. Both engineered strains in the ancestral M background retained the M phenotype, but
299 both engineered strains in the M strain 5.8 background recapitulated the D transition that was observed
300 in strains 5.9a and 5.9b (Table 1). These results indicate that the two chimeric Wsp proteins require
301 additional mutation(s) observed within this lineage to produce c-di-GMP. Both the WspA::D and
302 WspB::D chimeras have lost WspC, which is not surprising since the methylation sites of WspA were
303 removed previously in D strain 5.3. Similarly, WspB is completely removed in the WspA::D chimera and
304 nearly 75% of WspB has been removed in the WspB::D chimera. At this stage, it remains unclear
305 whether or not the observed mutations in *ilvH* and/or *parA* are required for the function of the two Wsp

306 chimeras. However, we present additional evidence below that strengthens the relationship between
307 IlvH and the Wsp system.
308 The WspB::D chimera strain 5.9b was next used to evolve M progeny strains. Sister strains 5.10a
309 and 5.10b were isolated and each were found to carry frameshift deletions in *ilvI* that decreased c-di-
310 GMP levels (Fig. 4). The two *ilvI* mutants carry a deletion of 17 or 23 nucleotides that start at the same
311 position, which should abolish IlvI's function by causing a frameshift. IlvI and IlvH form a complex that
312 catalyzes the first step of BCAA biosynthesis, where IlvH serves as the regulatory subunit and IlvI serves
313 as the catalytic subunit [39]. IlvH in *E. coli* has been bioinformatically predicted to respond to c-di-GMP
314 levels due to the presence of the inhibitory I-site [37], which we also detected in most DGCs (Fig. 5). We
315 identified that IlvH of *P. fluorescens* Pf0-1 also contains the I-site RXXD motif at residues 103-106. None
316 of the independently identified IlvH mutations (A36E, S149R, and G150S) in our study fall within this
317 motif, but all three mutations significantly increase c-di-GMP levels (Fig. 6). Beyond the potential
318 allosteric regulation of IlvH by c-di-GMP, there is no known relationship between BCAA biosynthesis and
319 c-di-GMP production to the best of our knowledge. However, we suspected that the IlvH mutations,
320 including the G150S mutation observed earlier in this lineage, increase BCAA production to stimulate c-
321 di-GMP production through an unknown mechanism, since we subsequently observed frameshift
322 mutations in the catalytic subunit (IlvI) that returns this lineage back to the M phenotype with reduced
323 c-di-GMP levels.
324 The frameshift mutations in *ilvI* should lead to BCAA auxotrophy, which is likely masked by the
325 nutrient-rich medium utilized in our experimental evolution system. To test this prediction, we grew
326 strains 5.10a and 5.10b in a chemically defined minimal medium without BCAA. We did not observe any
327 growth unless BCAA was exogenously supplemented (Fig. S3), confirming that our *ilvI* mutants are
328 unable to synthesize BCAA. We next tested if exogenous supplementation of BCAA alone could restore
329 c-di-GMP production in the *ilvI* mutant (M strain 5.10a). Since the *ilvI* mutant cannot grow in the

330 minimal medium without BCAA supplementation, we also included our prototype M and D ancestors
331 (Fig. 1A) as relative controls in addition to the *ilvH* mutant (D strain 5.7) and the *parA* mutant (M strain
332 5.8) from the same lineage. Exogenous supplementation of BCAA in the *ilvI* mutant indeed restored c-di-
333 GMP production at comparable levels to both D and the *ilvH* mutant (D strain 5.7) (Fig. 7). In contrast, c-
334 di-GMP levels remained the same in both M and the *parA* mutant (M strain 5.8) regardless of BCAA
335 supplementation (Fig. 7). These results show that overabundance of BCAA does not correlate with c-di-
336 GMP production and defeats our initial prediction that the missense mutations in *ilvH* increase BCAA
337 production to stimulate c-di-GMP production. Although BCAA supplementation restores c-di-GMP
338 production in the *ilvI* mutant strain in the minimal medium, the reduction of c-di-GMP levels observed in
339 the same *ilvI* mutant under our nutrient-rich experimental evolution conditions (Fig. 6) is not likely
340 associated with losing the ability to synthesize BCAA. Accordingly, reconstructing the two frameshift *ilvI*
341 mutations independently in the ancestral D strain did not cause a shift to the M phenotype, but the
342 initially observed shift to the M phenotype was recapitulated when these mutations were introduced
343 into their direct parental D strains (Table 1). Since IlvI forms a complex with IlvH, the observed
344 frameshift mutations in *ilvI* likely decouple the complex, and consequently impact IlvH's potential
345 function to modulate c-di-GMP production. Lineage five returns to the D phenotype in four sister
346 branches following the *ilvI* mutations through mutations in *wspE* or *dcgH* (Fig. 4). As already discussed
347 above, we commonly observe activating *wspE* mutations when the upstream signaling Wsp components
348 are disrupted, and the in-frame deletion in *dgcH* is also identical to the deletion reported in the D strain
349 4.1. These four independent transition steps into the D phenotype clearly indicate that the catalytic
350 activity of IlvI is not required for c-di-GMP production.

351 Lineage 27 was commenced with an engineered *ΔwspCD* M strain (Table S1, strain 27.0), where
352 we also observed the shift to the D phenotype through a missense mutation in IlvH (A36E) by restoring
353 c-di-GMP production (Fig. 6). In contrast to the M-shifting ParA (D115N) mutation that followed the D-

354 shifting IlvH (G150S) mutation in lineage 5, the transition from IlvH (A36E) to the M phenotype was
355 associated with a mutation which converts the stop codon of *wspB* with a cysteine residue to extend its
356 open reading frame, but out of frame with *wspE* (both *wspC* and *wspD* were already deleted). A
357 common trend exists between lineages 5 (Fig. 4) and 27 (Table S1) in that multiple mutations first occur
358 in Wsp proteins, which is proceeded by mutations in a non-Wsp DGC (SadC or DgcH, respectively), then
359 unique missense mutations occur in IlvH to stimulate c-di-GMP production. Reconstructing the three
360 IlvH missense mutations in the ancestral M strain does not lead to a shift to the D phenotype, but
361 reconstructing these mutations in their direct parental M strain recapitulates the initially observed shift
362 to the D phenotype (Table 1). The common targets of mutations between the two lineages that
363 converge on IlvH mutations are Wsp proteins, which implies that the c-di-GMP stimulating mutations in
364 IlvH specifically associate with a de-regulated Wsp system. Furthermore, the undoing of the IlvH (A36E)-
365 induced c-di-GMP production by the stop codon mutation in *wspB* implies potential IlvH-Wsp
366 interactions that are unlikely to be purely metabolic in nature.
367

368 **A macro assessment of sequential mutation patterns across all 33 parallel lineages captures potential**
369 **associations within the c-di-GMP regulome**

370 A long-standing question in the field is why microbes possess so many independent DGC and/or
371 PDE machineries. A systematic mutational analysis of genes that were bioinformatically predicted to be
372 DGCs in *P. fluorescens* demonstrated that most have little impact on the intracellular c-di-GMP pool [9],
373 and a significant number of DGCs/PDEs in *E. coli* are present in an inactive form [8]. In addition,
374 independent DGCs could regulate a sub-cellularly localized role [40] that could also contribute to the
375 total intracellular pool to regulate diverse physiological pathways across a gradient [41]. Our study
376 indicates that many known or predicted DGCs could be independently stimulated to regulate a common
377 phenotypic shift, which appears to operate across a broad range of c-di-GMP levels (Fig. 1C). We also

378 captured mutations in genes with no previously known associations with c-di-GMP moduclation that
379 significantly impact the c-di-GMP pool, and these genes are affected repeatedly across multiple lineages
380 (Table S1), which strongly suggests that they are indeed components of the c-di-GMP regulome. To
381 visualize patterns of sequential mutations and potential associations within the c-di-GMP regulome, we
382 compiled all sequential orders of the mutation events across the 33 parallel lineages into a single node-
383 edge plot [42] (Fig. 8A). The nodes represent the mutated genes in our experiment. The edges (i.e. lines)
384 of the plot report if the mutation causes an M (blue) or D (orange) phenotype, and the thickness of the
385 edge reflects the frequency of the observed pattern (Table S2). Proteins that are integrated into this plot
386 – meaning that many edges connect to a specific node – collectively form the main ring. Nodes
387 associated with a single edge fall out of this ring, and mutations in these proteins typically occur at the
388 end of a lineage or a branched sub-lineage that was not sequenced. Since we did not isolate any
389 progeny strains from these ten mutants that fall outside the main ring, we will not discuss them further.
390 The largest nodes in Fig. 8A are represented by Wsp proteins, DgcH, and other known DGCs like
391 YfiN, GcbC, MorA, and SadC. We observe that mutations in WspA that increase c-di-GMP are primarily
392 followed by mutations in WspB, WspD, or WspE that result in the M phenotype (blue edge) with
393 decreased c-di-GMP. Mutations in WspF that fail to return the Wsp system back to the ground state are
394 followed by mutations in WspC to abolish WspA's activity, mutations in WspA to force an off
395 conformation, or mutations in WspR to physically shut down c-di-GMP production. The frequency of
396 these patterns correlates well with the direction of signal flow in the Wsp system (Fig. 3), where the
397 primary mutations constitutively activate the Wsp system and subsequent mutations disrupt the signal
398 relay among the downstream components. Then, activating mutations occur in WspE that decouple
399 WspE from the upstream components to restore c-di-GMP production, which is followed by mutations
400 in WspE that deactivate it or mutations in WspR to shut down c-di-GMP production. The majority of
401 DGCs like SadC and YfiN have blue recursive edges that cause an M phenotype, which indicates that

402 mutations occur in the same protein to shut down its activity, immediately following a mutation that
403 initially stimulated its activity. The high frequency of blue recursive edges associated each DGC and
404 yellow edges between distinct DGCs collectively indicate that each DGC simply replaces another to
405 restore c-di-GMP production. Blue edges between DGCs are extremely rare, which suggests that
406 individual DGCs do not directly interact with another. Notably, there are several proteins with both
407 yellow and blue edges that are integrated in this plot and have not been shown to have a role in c-di-
408 GMP regulation or production. We next infer potential function of these proteins with respect to c-di-
409 GMP modulation.

410 ***NarA*** (N-ethylammeline chlorohydrolase associated c-di-GMP regulator): In strain 2.3, we
411 observe that the A383S mutation in NarA increases c-di-GMP levels (Fig. 8B), which confirms that this
412 hypothetical protein is indeed biologically active. This NarA mutation follows the M-shifted W90L
413 mutation in WspD, which suggests that NarA is either able to restore Wsp signaling or activate other
414 DGCs to increase c-di-GMP levels. We have no reason to suspect that NarA directly catalyzes c-di-GMP
415 since it lacks any c-di-GMP associated domains or motifs. The progeny of this NarA mutant carries a
416 nonsense mutation in *wspD*, reverting this strain back to an M phenotype (Table S1). Thus, the A383S
417 mutation in NarA associates specifically with *wspD* mutations to both restore and shut down c-di-GMP
418 production. NarA is predicted to catalyze N-ethylammeline, a derivative of ammeline, and a recent study
419 theorized that ammeline is likely an essential building block required for the synthesis of cyclic
420 complexes [43]. Although the metabolic connections are unknown, there is a strong indication that NarA
421 interacts with WspD at some capacity to modulate c-di-GMP levels.

422 ***CdrB*** (Two-partner secretion system transporter): Pfl01_0652 in *P. fluorescens* encodes a protein
423 that is homologous to the transporter protein CdrB in *P. aeruginosa* (PA4624). In *P. aeruginosa*, CdrA
424 and CdrB are encoded in a single operon and form a two-partner secretion (TPS) system associated with
425 biofilm formation [44]. CdrA (c-di-GMP regulated TPS A) is an extracellular adhesin known to respond to

426 modifications made by the periplasmic protease LapG which is activated by the transmembrane c-di-
427 GMP receptor LapD [45]. It has been reported that high intracellular levels of c-di-GMP enable CdrA to
428 bind and crosslink secreted Psl, thereby increasing cell-cell adhesion [44]. *cdrA/B* expression also
429 increases proportionally with intracellular levels of c-di-GMP during biofilm formation [46]. CdrB is a
430 transporter with domains that indicate it is a type V secretion system transporter. CdrB is likely involved
431 in the transport of the adhesin CdrA but has no identified role in c-di-GMP modulation. In our lineage 6,
432 the missense mutation YfiN (G157C) increases c-di-GMP production, which is immediately followed by
433 the CdrB A290T missense mutation to decrease c-di-GMP levels (Fig. 8B). This suggests that an unaltered
434 CdrB or its native transport activity is necessary for YfiN's DGC activity. As reported in Table S1,
435 mutations that follow the CdrB mutation occur in *morA* or *dgcH*, each increasing c-di-GMP as indicated
436 by the D-phenotype (Table S1). Therefore, the negative impact of our CdrB mutation on YfiN could be
437 recovered through the genetic activation of other DGCs, which could also reflect interactions with CdrB.
438 ***DgcX* and *DgcY*** (Bioinformatically predicted DGCs): Pfl01_3550 and Pfl01_3508 are both
439 bioinformatically predicted to encode DGCs, but their enzymatic function has not yet been
440 demonstrated. Here, we establish that they are both functionally active in c-di-GMP catalysis and
441 annotate them as *dgcX* and *dgcY*, respectively, since proteins DgcA through DgcW already exist.
442 Pfl01_3550, hereon *dgcX*, is a commonly mutated gene in our dataset which increases c-di-GMP (Table
443 S1). We observe a blue recursive loop in the node-edge plot for DgcX, which is consistent with other
444 known DGCs (Fig. 8A). We isolated two independently evolved D mutants with the same M350I
445 mutation, and an M mutant with an in-frame deletion of L289. Phenotypic and motility data support
446 that the observed mutations in *dgcX* influence the intracellular c-di-GMP pool. The genomic location of
447 *dgcY* is in a region of hypothetical genes that appear to form an operon. Interestingly, our *dgcY* mutant
448 strains carry large deletions that span the 9 hypothetical genes within this genomic region (Fig. 5). The
449 deletion of Pfl01_3505, Pfl01_3506, and the 5' UTR region of *dgcY* results in a significant increase in c-di-

450 GMP (Strain 6.5a, Fig. 8B), which likely replaces the native promoter region of *dgcY* with that of
451 Pfl01_3505. C-di-GMP is significantly decreased in the progeny strain 6.6a (Fig. 8B) after the deletion of
452 Pfl01_3500, Pfl01_3501, Pfl01_3502, Pfl01_3503, Pfl01_3504, Pfl01_3505, Pfl01_3506, Pfl01_3508,
453 Pfl01_3509, and Pfl01_3510, which includes *dgcY*. It is unclear whether or not the encoded proteins of
454 the hypothetical genes that flank *dgcY* are functionally related to DgcY. We had initially suspected that
455 these hypothetical genes could encode a complex signal transduction system like Wsp, but we did not
456 detect any homologous Wsp domains or other c-di-GMP associated motifs.

457 ***CalM*** (c-di-GMP associated LysM): The hypothetical gene Pfl01_1895, hereon *calM* (c-di-GMP
458 associated LysM) is a commonly mutated gene in our study (Table S1). The encoded protein contains
459 domains with homology to the LysM peptidoglycan-binding superfamily and contains a FimV C-terminal
460 transmembrane domain that is implicated in modulating motility [47,48]. The LysM proteins are
461 identified by the lysin motif which is associated with cell lysis. The presence of the LysM and FimV
462 domains suggests that this protein may respond to changes in peptidoglycan stress, which is essential
463 for maintaining cell shape and integrity. C-di-GMP is a well-known regulator of cellular morphology in
464 *Vibrio cholera* and *Caulobacter crescentus* [13,49]. In addition, surface-sensing through the Wsp system
465 in *P. aeruginosa* was recently demonstrated to be associated with cell envelope stress [28]. We observe
466 a duplication of five nucleotides within *calM* that results in a significant decrease in c-di-GMP (Fig. 8B).
467 Two repetitive clusters of CAGCG shifts to three clusters to cause a frameshift. This mutation follows a
468 *dcgH* in-frame deletion that dramatically increases c-di-GMP production, indicating that CalM is
469 necessary for DgcH's activity. Remarkably, three independently evolved progeny strains in this lineage
470 carry mutations that remove the initial five nucleotide insertion, returning each strain back to the D
471 phenotype likely by restoring DgcH's activity (Table S1).

472 ***RndA*** (RND transporter): Pfl01_2749 is bioinformatically predicted to encode an RND
473 transporter. RND transporters function as efflux pumps to remove toxins, antibiotics, quorum sensing

474 (QS) molecules, and other metabolites [50]. We observed that the nonsense mutation Q51* in
475 Pfl01_2749, hereon *rndA*, significantly decreases c-di-GMP levels (strain 11.2, Fig. 8B). A recent study
476 speculates that QS molecules contribute to a feedback loop to inhibit c-di-GMP production [51]. Thus,
477 an active RndA could potentially modulate this feedback loop by expelling certain effector compounds
478 to stimulate c-di-GMP production. The *rndA* mutant shifts to the D phenotype through an in-frame
479 deletion that removes amino acid residues 524-537 in DgcH. This specific mutation was observed in
480 multiple lineages to exclusively stimulate c-di-GMP production.

481 To confirm whether the observed mutations in these atypical c-di-GMP associated genes alone
482 could modulate c-di-GMP levels, we reconstructed representative mutations in their respective
483 ancestral backgrounds. None of the engineered strains produced a phenotypic shift (Table 1), indicating
484 that specific mutations in DGCs are first required to impact c-di-GMP levels. Accordingly, reconstructing
485 the same mutations in their direct parental strains recapitulates the initially observed phenotypic shifts
486 (Table 1). Although functional studies are required to prescribe specific mechanisms, diverse cellular
487 processes appear to be integrated with numerous catalytic machineries to modulate the c-di-GMP pool
488 in *P. fluorescens*, and the missense and in-frame deletion mutations observed in Wsp proteins and other
489 DGCs (Fig. 5) could reflect potential interaction sites.

490

491 **Conclusion**

492 Although we have extensive knowledge on how specific enzymes make or break c-di-GMP and
493 how this molecule interacts with a large number of regulatory elements to modulate diverse
494 physiological processes, relatively little is known about how C-di-GMP production itself is regulated. This
495 study takes advantage of a repeatedly evolving social trait in *P. fluorescens* to demonstrate how
496 numerous proteins could independently and collectively produce remarkable sequences of genetic
497 innovation to oscillate c-di-GMP levels. Our extensive library of *wsp* mutations allows us to reinforce the

498 current model of the Wsp system, which heavily draws functional analogies to the *E. coli* chemotaxis
499 system and particularly lacks domain resolution in WspB and WspD [17]. Beyond the Wsp system, we
500 have identified unique missense and in-frame deletion mutations in multiple DGCs that fall outside their
501 conserved catalytic domain. These mutations likely reflect regulatory domains that are critical for
502 modulating enzymatic activity. We have also confirmed that several bioinformatically predicted DGCs to
503 be indeed enzymatically active. In particular, DgcY is encoded within a nine gene cluster of unknown
504 function. Although we could not identify any specific homologies, the large deletions we observed in this
505 cluster lead us to speculate that they encode a unique system that functions to regulate DgcY's activity.
506 We have also uncovered a set of unexpected or hypothetical proteins that clearly have the
507 capacity to influence c-di-GMP turnover. Three missense mutations in *ilvH* were identified to
508 independently stimulate c-di-GMP production, which appears to be independent of IlvH's primary role in
509 BCAA biosynthesis, but rather operates through an unknown interaction with the Wsp system. We have
510 identified the same I-site in IlvH as in most DGCs, which suggests that IlvH physically interacts with c-di-
511 GMP. Similarly, CalM, CdrB, and RndA homologs in other organisms have been implicated to respond to
512 c-di-GMP levels, but they have never been associated with modulating c-di-GMP production. We have
513 confirmed that the mutations observed in these proteins alone do not impact c-di-GMP levels, but do so
514 in the presence of genetically modified DGCS or the Wsp signal transduction system. In particular, a
515 DgcH-driven c-di-GMP production is negated by a frameshift mutation in *calM*, which implies a potential
516 interaction between these two proteins. Similarly, a YfiN-driven c-di-GMP production is negated by a
517 missense mutation in *cdrB*, and c-di-GMP production appears to be restored again through a mutation in
518 either *morA* or *dgcH*. Furthermore, a *narA* missense mutation is flanked in sequence by independent
519 mutations in *wspD* to modulate c-di-GMP production in both directions.
520 An emerging concept here is that the intracellular pool of c-di-GMP, whether it be subcellularly
521 localized or in sum, appears to be modulated through the catalytic activities of many independent DGCs

522 that are in tune with diverse proteins. Such intricacies are masked by the activities of DGCs with high
523 output, but they are clearly hardwired in the genome. Although direct functional studies are necessary
524 to resolve the underlying mechanisms, this study reveals a complex and underappreciated
525 interconnectivity within the c-di-GMP regulome of *P. fluorescens*. Similar relationships could also
526 manifest in other *Pseudomonas* and related species that share the same DGCs and other proteins
527 described in this study. In particular, very little is known about the functional domains of most DGCs
528 beyond their conserved catalytic domain. The vast majority of the missense mutations or in-frame
529 deletions captured in this study occur outside of the catalytic domain to clearly activate or shut down c-
530 di-GMP production. Our extensive library of functionally important mutations presented here should
531 facilitate mechanistic studies of phylogenetically conserved DGCs that remain heavily under-explored.
532

533 **Material and Methods**

534 **Strains and culture conditions**

535 All *Pseudomonas fluorescens* Pf0-1 [52] derivatives associated with parallel experimental
536 evolution are described in Table S1 and engineered strains are described in Table 1. Strains were
537 routinely grown in Lennox LB (Fisher BioReagents), *Pseudomonas* Minimal Medium (PMM) [53], or on
538 *Pseudomonas* Agar F (PAF) (Difco). *Pseudomonas* F (PF) broth (a non-agar variant of PAF) was prepared
539 with the following: pancreatic digest of casein 10 g/L (Remel), proteose peptone No. 3 10 g/L (Remel),
540 dipotassium phosphate 1.5 g/L (Sigma-Aldrich), and magnesium sulfate 1.5 g/L (Sigma-Aldrich). Cultures
541 were incubated at 30°C and shaken at 250 rpm when applicable.

542 **Parallel experimental evolution**

543 Pure cultures of the ancestral M strain or engineered M strains were grown overnight in 5mL LB
544 broth and 25uL volumes were spotted on PAF plates, then incubated at room temperature for 3 to 8
545 days to allow spreading fans to emerge. To ensure consistency across experiments, PAF plates were

546 always prepared and left to dry at room temperature for 2 days before being inoculated. One fan was
547 randomly sampled from each colony and streaked out on LB plates in duplicate. Sampling a fan always
548 produced two strains with either a mucoid (M) or dry (D) colony phenotype. A single isolated colony
549 exhibiting the D phenotype was randomly selected to start a new liquid culture and also frozen down.
550 This process was repeated to sample six independent fans (i.e. six lineages). Three of the six
551 independently isolated D strains were randomly selected and cultured as above to start the next round
552 of experimental evolution. We repeated the same sampling process as above except that new M
553 phenotypes were isolated instead. We bidirectionally selected M and D phenotypes for as many as 13
554 rounds for a single lineage, but the number of sampled fans at each step was reduced over time in a
555 varying manner across independent lineages. In total, approximately 600 independently evolved isolates
556 were frozen down across 33 parallel lineages. Every isolate was subjected to a motility assay in an LB
557 plate with 0.25% agar, and the prototype M and D ancestors were used as controls [24]. In addition,
558 25uL of pure cultures of each isolate, the ancestral strain with the opposite phenotype, and a 1:1
559 mixture of both were spotted onto PAF plates in triplicate and assessed for cooperative radial spreading
560 (Fig. 1A) to filter out hyper-motile and non-cooperative mutants [24]. Colony diameters were measured
561 and recorded after four days of incubation at room temperature and considered cooperative if the
562 measured diameter of the 1:1 colony exceeded both the diameters of the isolated mutant strain and the
563 respective ancestral strain. Isolates that failed this test were removed from this study.

564 **Reconstruction of naturally derived mutations in ancestral and direct parental backgrounds**

565 Experimentally evolved isolates were whole genome sequenced to identify the causal mutations
566 as described below. We reconstructed select naturally acquired mutations in the respective ancestral
567 background and also in the direct parental background using previously described methods [24]. PCR
568 primers were developed from the sequence data to amplify mutations of interest and are reported in
569 Table S3. Isolates were grown overnight and underwent DNA extractions (Qiagen). Dream Taq DNA

570 Polymerase (ThermoFisher) was used in PCR reactions with purified DNA to generate insert fragments
571 carrying the mutations which ranged in size from 456bp to 934bp. PCR was carried out using the
572 recommended conditions of the Dream Taq amplification kit for amplicons below 2000bp. Inserts were
573 cloned into the pGEM-T Easy vector system (Promega) and then subcloned into the *Not*I site of the
574 suicide plasmid pSR47s [54]. Suicide plasmids were heat shocked into *E. coli* S17.1λ*pir*, mated with the
575 target strains reported in Table S3 on LB plates at 30°C for 16 hours, then plated onto PMM plates
576 supplemented with 50 ug/ml kanamycin. We observed that *ilvI* mutants could not grow on PMM and
577 therefore replaced the PMM selection plate with an LB plate supplemented with 50 ug/ml kanamycin
578 and 100 ug/ml ampicillin for *ilvI* mutant constructs. Isolated colonies were grown overnight, serially
579 diluted and plated out on LB plates supplemented with 15% sucrose (w/v) for counterselection. Isolated
580 colonies were placed in cryo-storage as described above. Crude DNA extracts were made for each strain
581 where 100uL of overnight culture was boiled at 100°C, centrifuged at 15,000 RCF for 30 seconds, and
582 10uL of supernatant was used for PCR using the primers reported in Table S3. PCR products underwent
583 gel extraction and subsequent sanger sequencing (primers in Table S3) to confirm that the mutation was
584 successfully engineered into the target strain. Upon PCR confirmation, pure cultures of cells from cryo-
585 storage underwent DNA extraction (Qiagen) and were submitted for WGS which confirmed that no
586 additional mutations had accumulated in the target strains during mutant construction.

587 **DNA extraction, whole genome sequencing, and variant calling**

588 Pure cultures were grown overnight in 5mL LB broth at 30°C. 1 mL was spun down to form a
589 pellet for DNA extraction. Pelleted cells were mechanically lysed with the Qiagen TissueLyser LT at 50
590 oscillations/second for 10 minutes. The Qiagen DNeasy UltraClean Microbial DNA extraction kit was
591 used following the standard operating procedures. Samples were then eluted into 30uL H_2O after a 5
592 minutes incubation at 4°C with the elution media and stored at -20°C prior to shipment. Genomic DNA
593 library preparations were carried out by the Microbial Genome Sequencing Center (Pittsburgh, PA)

594 following standard operating procedures. Pooled and indexed samples were sequenced on the NextSeq
595 2000 platform and demultiplexed prior to data delivery. The Trimmomatic algorithm was used to group
596 and quality filter paired reads at a Phred score of 20 using a 4bp sliding window. The BreSeq algorithm
597 was used to align the paired reads to the *P. fluorescens* Pf0-1 reference genome (CP000094.2) and
598 evaluate for single nucleotide polymorphisms (SNPs), insertions, deletions, or rearrangements. Output
599 sequence data from BreSeq is compiled as 'Table S1 – Source Data 1' and was manually evaluated for
600 each strain to determine the order of mutations for a given lineage.

601 **Alignment of mutation data to annotated domains**

602 Domain analyses of Wsp proteins and DGCs were conducted and rendered as previously
603 described [17]. Peptide sequences of the predicted or known DGCs were obtained from the
604 *Pseudomonas* Genome Database [55]. NCBI's conserved domain database (CDD) was used to evaluate
605 the functional domains [56]. Mutation data of Wsp proteins from this study were manually mapped to
606 the rendered consensus sequence of the respective Wsp protein [17].

607 **C-di-GMP extraction and LC-MS/MS**

608 An isolated colony of each strain was transferred to PF broth and grown overnight. Overnight
609 cultures were diluted to an OD_{600} of 0.04 in triplicate and incubated for 2-4 hours until the samples
610 reached an OD_{600} of 0.5, then promptly processed for c-di-GMP extraction. C-di-GMP extraction and
611 quantification procedures followed the protocols established by the Michigan State University Research
612 Technology Support Facility (MSU-RTSF): MSU_MSMC_009 protocol for di-nucleotide extractions and
613 MSU_MSMC_009a for LC-MS/MS, with the following modifications. All the steps of c-di-GMP extraction
614 were carried out at 4°C unless noted otherwise. 1mL of 0.5 OD_{600} culture was centrifuged at 15,000 RCF
615 for 30 seconds, and cell pellets were resuspended in 100uL of ice cold acetonitrile/methanol/water
616 (40:40:20 (v/v/v)) extraction buffer supplemented with a final concentration of 0.01% formic acid and
617 25nM c-di-GMP-Fluorinated internal standard (InvivoGen CAT: 1334145-18-4). Pelleted cells were

618 mechanically disturbed with the Qiagen TissueLyser LT at 50 oscillations/second for 2 minutes.
619 Resuspended slurries were incubated at -20°C for 20 minutes and pelleted at 15,000 RCF for 15 minutes
620 at 4°C. The supernatant was transferred to a pre-chilled tube then supplemented with 4uL of 15% w/v
621 ammonium bicarbonate (Sigma-Aldrich) buffer for stable cryo-storage. Extracts were stored at -80°C for
622 less than two weeks prior to LC-MS/MS analysis at MSU-RTSF. Sample degradation was observed with
623 repeated freeze-thaw cycles, so extracts were never thawed until LC-MS/MS analysis. All samples were
624 evaporated under vacuum (SpeedVac, no heat) and redissolved in 100uL mobile phase (10 mM TBA/15
625 mM acetic acid in water/methanol, 97:3 v/v, pH 5). LC-MS/MS quantification was carried out with the
626 Waters Xevo TQ-S instrument with the following settings: c-di-GMP-F at *m/z* transition of 693 to 346
627 with cone voltage of 108 and collision voltage of 33; c-di-GMP at *m/z* transition of 689 to 344 with cone
628 voltage of 83 and collision voltage of 31. C-di-GMP data was normalized to 25nM c-di-GMP-F by MSU-
629 RTSF to account for sample matrix effects and sample loss during preparation. OD_{600} measurements of
630 the initial samples were used to report the quantified c-di-GMP as nM/OD and visualized with GraphPad
631 Prism9.

632 **BCAA supplementation assay and c-di-GMP quantification**

633 Pure cultures were grown overnight in 5mL LB broth. 5uL of each culture was transferred into
634 5mL PMM. Cultures were supplemented with the BCAA valine, leucine, and isoleucine as previously
635 described [57]. Assessment of growth during BCAA supplementation contained either 0uM (loading
636 control), 180uM, 200uM, 220uM, 250uM, or 300uM in triplicate. Samples were incubated at 30°C for 24
637 hours at 250 rpm shaking. Cultures were manually pipetted to resuspend cells and 300uL of culture was
638 transferred to a 96-well black wall clear bottom plate for OD_{600} quantification. OD was quantified using
639 the SpectraMax plate reader and background (determined from blanks) was removed from each
640 quantified sample. Data analysis and visualization of growth during BCAA supplementation was
641 conducted in Excel. To evaluate the relationship between BCAA and c-di-GMP, pure cultures were grown

642 for 24 hours at 30°C and 250 rpm shaking in PMM liquid media containing either 0uM, 50uM, 100uM or
643 150uM of supplemented BCAAs. OD_{600} measurements were taken and samples were diluted to an OD_{600}
644 of 0.04 into PMM at the same BCAA concentrations. Samples were incubated for 24 hours under the
645 same conditions stated and then sonicated (Time 0.00:20, Pulse 01 01, Amplitude 20%) to disrupt cell
646 aggregates. OD_{600} measurements occurred every hour until OD_{600} was approximately equal to 0.25. C-di-
647 GMP analyte extraction was carried out as stated above with the modification that 2mL cultures were
648 used for cell lysis. Quantified values of c-di-GMP are reported as nM/OD_{600} and were visualized with
649 GraphPad Prism9.

650 **Node-edge analysis and visualization**

651 Data reported in Table S1 was used to generate the 'to-from' table which assesses mutation
652 patterns at the gene/protein level [42]. Counts were determined by the frequency of the to-from
653 patterns calculated from Table S1 where a mutation in a given gene/protein (to) occurred after a
654 mutation in another gene/protein (from). This table was uploaded to Cytoscape to visualize the nodes
655 (to genes/proteins) and edges (counts). Default renderings of the plot reported node centrality
656 (commonly mutated targets) through coordinate placement on the graph. This metric was converted to
657 node size with larger nodes representing more commonly mutated targets. Nodes were manually
658 aligned for visual clarity with nodes connected by two or more edges being placed in the main ring and
659 nodes with a single edge being placed outside the ring.

Figures and Tables

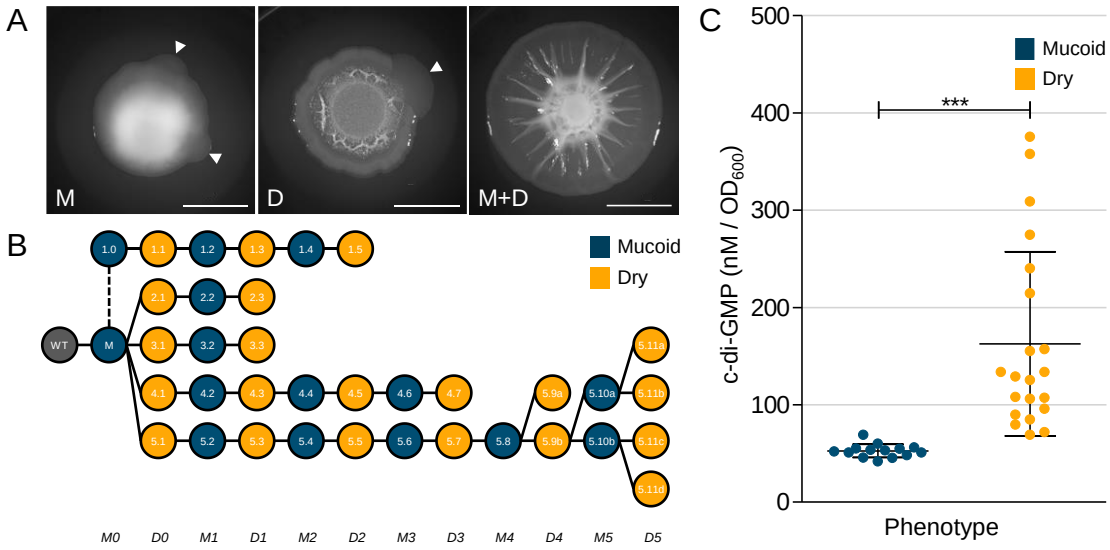

Figure 1. Bidirectional evolution of M and D phenotypes are c-di-GMP dependent. A) Colony morphologies of the ancestral mucoid (M, left) and dry (D, middle) strains after 4 days of growth. Arrows indicate the emergence of spreading fans that contain the respective parent strain and a new mutant strain with the opposite phenotype. The spreading phenotype is readily produced by artificially mixing M and D strains (right, scale bar = 10mm). B) Phylogeny of strains in select lineages colored by phenotype and corresponding colony morphologies are shown in Fig. S2. The numbers indicate the IDs of the evolved strains as shown in Table S1. Strain 1.0 was constructed from the ancestral M strain to lack the *wspC* gene, which encodes a methyltransferase known to activate the Wsp system. Each strain was isolated from naturally emerging fans from their respective parent colony with the opposite phenotype. This phylogeny depicts the bidirectional transitions between mucoid and dry states which we show are c-di-GMP dependent. C) C-di-GMP levels of evolved strains. C-di-GMP was quantified through LC-MS/MS and is reported as nM per OD600. Samples are categorized by phenotype and we report the triplicate mean ± SD for each phenotypic classification: mucoid n=14 and dry n=21 (*** Student's t-test $p < 0.001$).

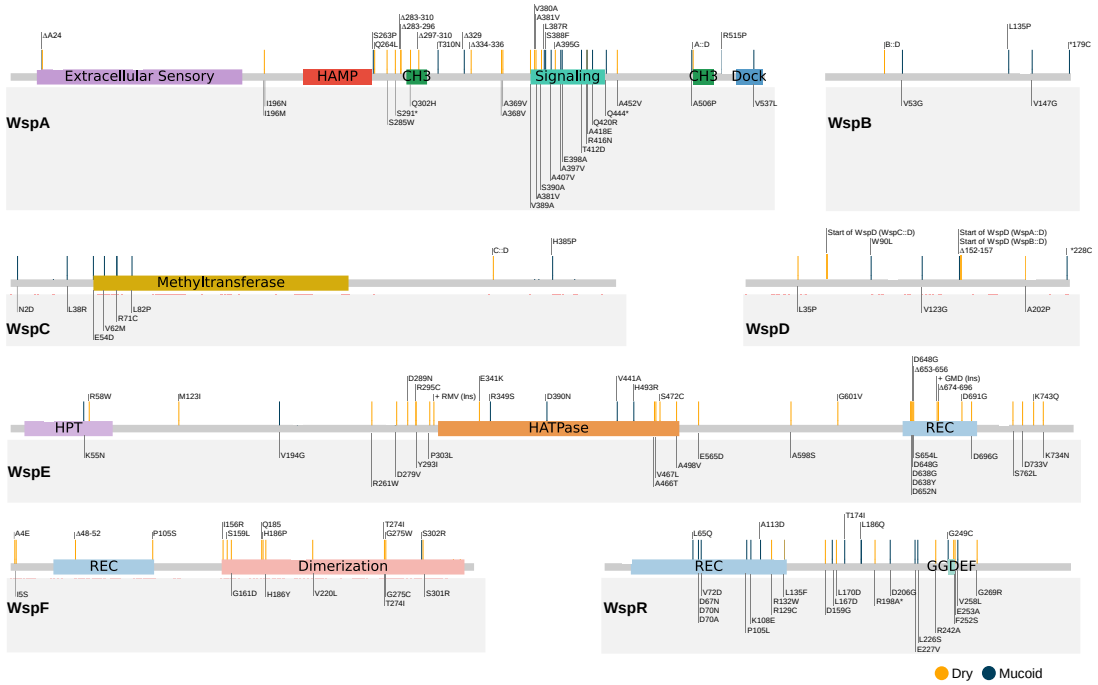

Figure 2. Alignment of our missense and in-frame deletion mutation data with previously annotated mutations in the Wsp system. Individual Wsp proteins are shown with their functional domains that were derived from CDD (NCBI), Prosite, or homology to the *E. coli* chemotaxis system (HAMP = transmembrane relay domain, CH_3 = methylation site, HPT = histidine phospho-transfer domain, HATPase = histidine kinase ATP binding domain, and REC = phosphoreceiver domain). Only the missense and in-frame mutations identified in this study are shown above each protein and they are mapped to the consensus sequence of each Wsp protein [17]. Previously annotated mutations [17] are shown within the gray box below each protein. Mutations indicated within the gray box are annotated to represent specific residues positions that were affected in the respective protein sequence of a given organism, but the grey horizontal bars indicate their actual positions within the consensus sequence. Therefore, the horizontal bar locations of the mutations identified in this study are directly comparable to previously identified mutations through the consensus sequence. Mutations that stimulate c-di-GMP production are indicated by orange horizontal bars and those that reduce c-di-GMP production are indicated by blue horizontal bars.

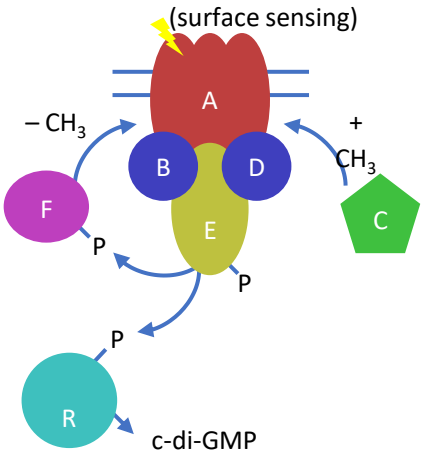

690

691 **Figure 3. Functional model of the Wsp signal transduction system.** The Wsp system in *P. aeruginosa*
692 responds to surface contact to ultimately produce c-di-GMP. (CH3 = methyl group, P= phosphoryl
693 group). Homology with the chemotaxis system predicts that once WspA is stimulated by surface-contact,
694 it undergoes a conformational change to expose cytosolic methylation helices that are necessary for
695 signal transduction [33]. The methyl-transferase WspC is then predicted to dock at the 5' tail of WspA
696 and methylate the WspA trimer-of-dimers complex [58]. The signal is then relayed through the coupling
697 proteins WspB and WspD, and subsequently to WspE, which functions as a histidine kinase [59]. WspE
698 phosphorylates the DGC WspR to stimulate c-di-GMP production [60]. Simultaneously, WspE
699 phosphorylates the methyl-esterase WspF, which de-methylates WspA and terminates the signaling
700 cascade [26]. Significant work has been carried out to characterize the biochemical functions of WspE
701 and WspR in particular, and WspE is a common mutational target in a clinical setting [17]. More
702 recently, studies have begun to explore the functional role of WspA during signal activation and
703 subcellular localization, revealing that both properties are dependent on WspB and WspD proteins
704 [27,61]. These studies also suggest that WspB and WspD likely possess unique functions, but they
705 remain unresolved.

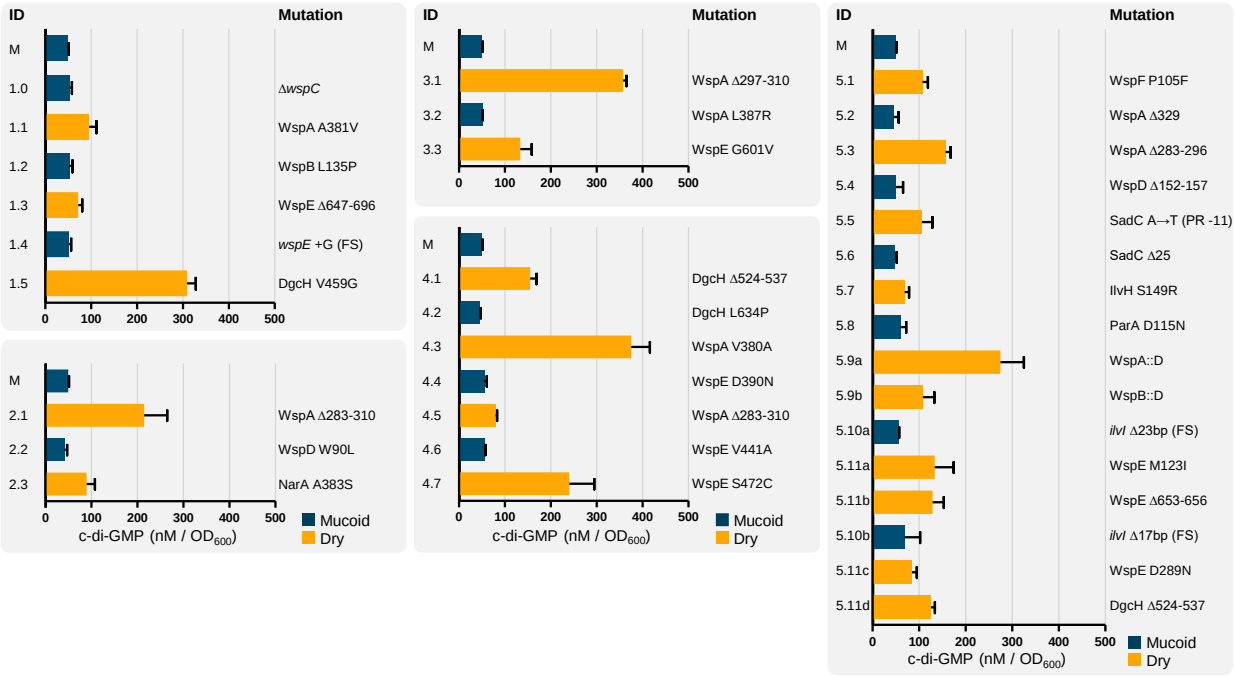

Figure 4. C-di-GMP oscillates between all M and D phenotypic transitions. C-di-GMP was quantified via LC-MS/MS and is reported as the triplicate mean ± SD. The charts capture the independently evolved strains within the five selected lineages shown in Figure 1B. D strains are shown in orange and M strains are shown in blue and their respective colony morphologies are shown in Fig. S2. The numerical IDs correspond to Table S1, and mutations reflect the affected amino acid residues, except frameshift (FS) and promoter region (PR) mutations refer to the specific nucleotides.

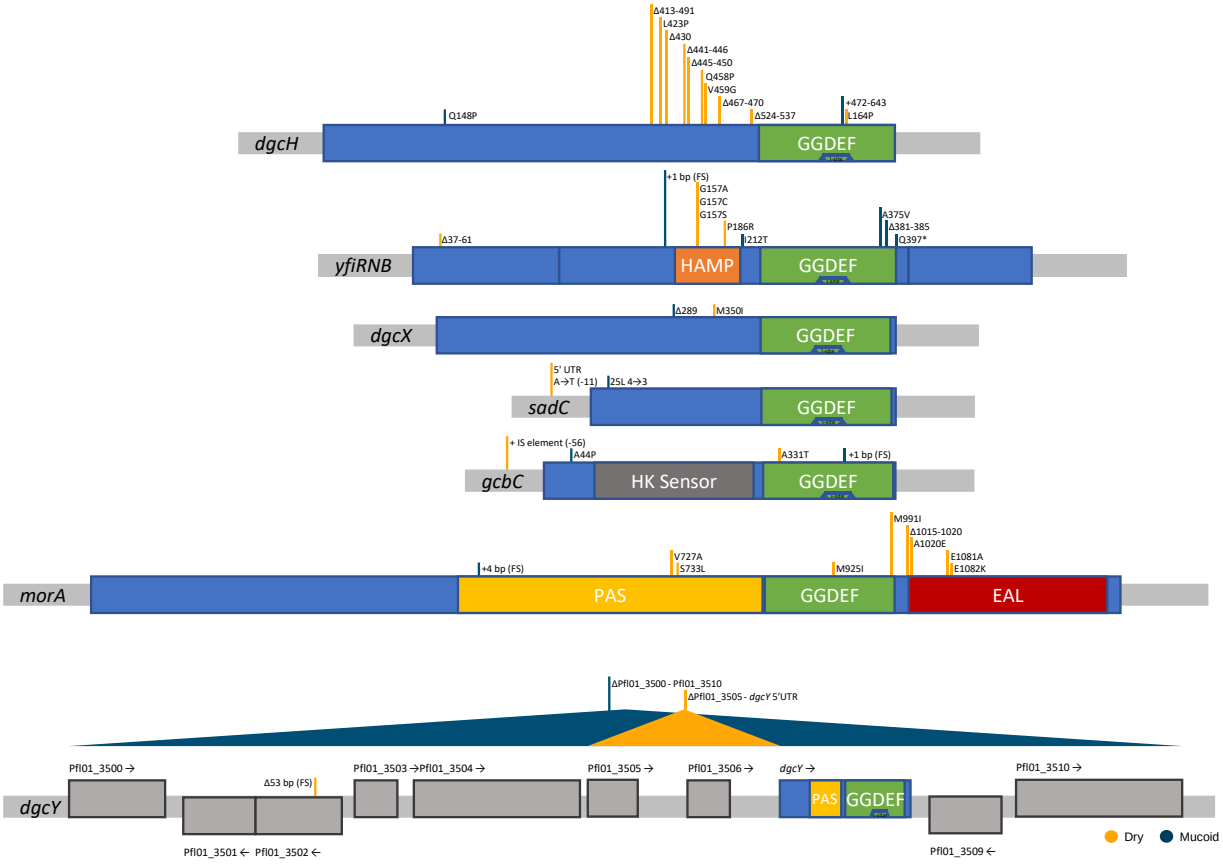

Figure 5. Alignment of our mutation data to annotated domains in known or predicted DGCs. Blue boxes represent the protein sequence and their flanking grey boxes represent untranslated regions. Each image represents a single DGC as indicated, with the exception of *yfiRNB* and *dgcY*. *YfiRNB* shows three blue boxes with each box representing YfiR, YfiN (DGC), or YfiB, respectively. *DgcY* shows a cluster of 10 genes with nine hypothetical genes of undetermined function and one bioinformatically predicted DGC (*dgcY*). Domain data were derived from CDD (NCBI): GGDEF = c-di-GMP catalytic domain, PAS = sensory signaling domain, EAL = phosphodiesterase hydrolysis domain, HAMP = transmembrane relay domain, I-site = c-di-GMP allosteric regulation site (shown inside GGDEF), HK Sensor = histidine kinase sensory domain. Mutations that stimulate c-di-GMP production are indicated by orange horizontal bars and those that reduce c-di-GMP production are indicated by blue horizontal bars.

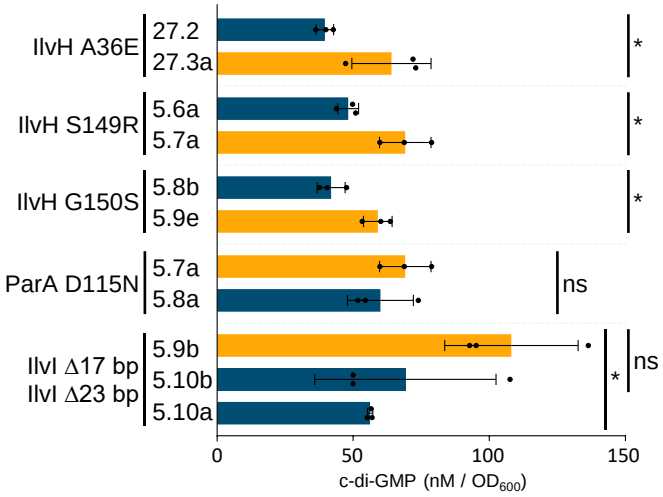

Figure 6. C-di-GMP levels fluctuate with BCAA mutations. C-di-GMP measurements in triplicate mean ± SD. Raw c-di-GMP values of each mutant and its respective parent are reported in Table S1. Causal mutation of each phenotypic shift is indicated on the left. D strains are shown in orange and M strains are shown in blue. (Student's t-test: ns = non-significant, * = $p < 0.05$).

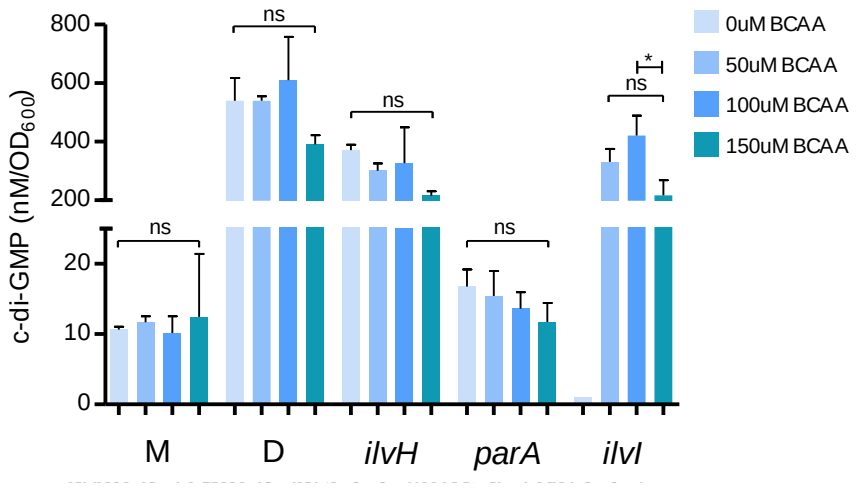

Figure 7. BCAA supplementation stimulates c-di-GMP production in a BCAA auxotroph with the M phenotype, but does not impact c-di-GMP production in non-BCAA auxotrophs with the same M phenotype. Strains were grown in the chemically defined PMM medium with 0, 50, 100, or 150 uM BCAA supplementation (valine, leucine, isoleucine). C-di-GMP was extracted and quantified via LC-MS/MS in triplicates and plotted as the mean with STD (ANOVA; Tukey's HSD Post Test: ns = non-significant, * = $p < 0.05$). M and D refer to the prototypical M and D strains in Fig. 1A. The *ilvH* mutant (D strain 5.7) produces c-di-GMP levels similar to the D strain control and the *parA* mutant (M strain 5.8) produces c-di-GMP levels similar to the M strain control. These relative patterns are consistent with the c-di-GMP quantification data reported in Fig 6 under nutrient-rich conditions. Exogenous supplementation of BCAA across all concentrations does not significantly impact c-di-GMP production. There is no data for the *ilvI* mutant at 0 uM BCAA, since this strain fails to grow in PMM unless BCAA is exogenously provided. However, the *ilvI* mutant (M strain 5.10a) produces c-di-GMP levels comparable to both D and the *ilvH* mutant (D strain 5.7) with BCAA supplementation.

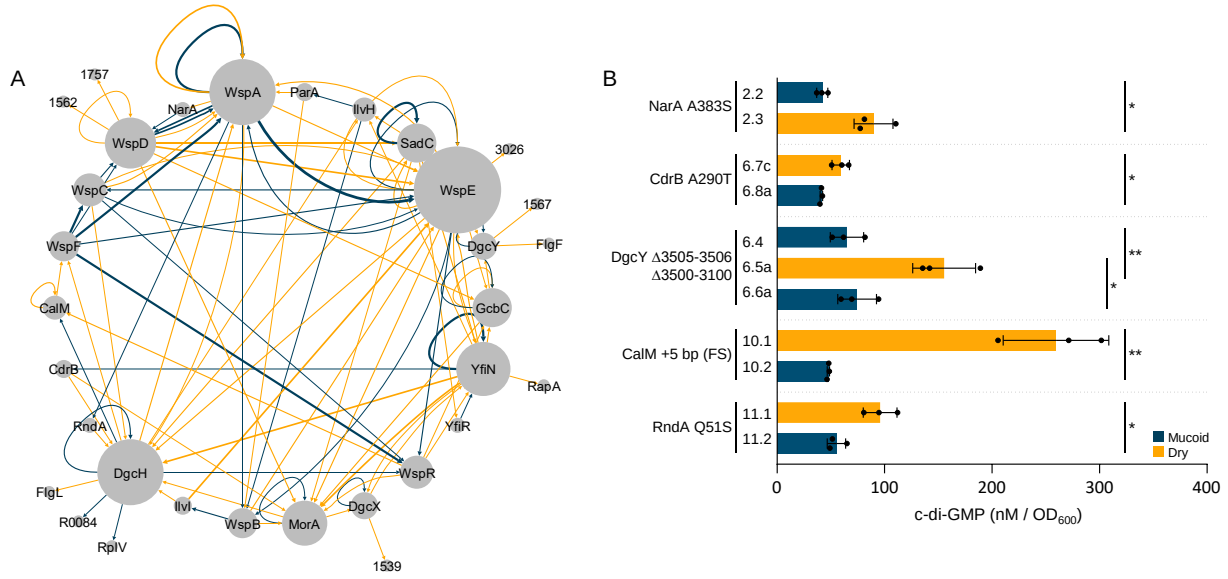

743

744 **Figure 8. A node-edge representation of 147 unique mutations across 33 lineages and c-di-GMP**

745 **quantification data of strains with mutations in proteins with significant network connectivity that are**

746 **not known to be associated with c-di-GMP modulation.** A) A node-edge plot reveals focal proteins

747 under selection. Each node represents a protein and each edge represents a relationship where one

748 mutation precedes or proceeds another. Orange edges represent M to D shifts and blue edges represent

749 D to M shifts. The relative size of a node and thickness of an edge is proportional to frequencies within

750 the dataset. Proteins that collectively form the ring represent commonly mutated targets in this study

751 and likely have a substantial role in c-di-GMP regulation. Proteins with limited connectivity fall outside

752 the main ring. B) LC-MS/MS validates that proteins with significant network connectivity, but not

753 previously associated with c-di-GMP, have a significant impact on intracellular c-di-GMP levels. C-di-

754 GMP measurements are reported as the triplicate mean ± SD. C-di-GMP values of each mutant and its

755 respective parent are summarized in Table S1 with the corresponding ID tag. D strains are shown in

756 orange and M strains are shown in blue. (Student's t-test: * = $p < 0.05$, ** = $p < 0.01$).

757 **Table 1. Reconstructing select naturally acquired mutations in both the ancestral and direct parent**

758 **strains reveal dependence on the previous mutation(s) to drive specific M-D phenotypic shifts.**

Strain ID	Strain Mutation	Mutation CDS ID	Mutant Phenotype	Parent Strain ID	Parent Strain Mutation	Ancestor ǂ	Reconstructed Mutants*	
							Parent	Ancestor
5.9a	WspA::D	Pfl01_1052::1055	dry	5.8a	ParA (D115N)	M	dry	mucoid
5.9b	WspB::D	Pfl01_1053::1055	dry	5.8a	ParA (D115N)	M	dry	mucoid
30.1	WspC::D	Pfl01_1054::1055	dry	Δ*rsmE*	Δ*rsmE*	M	dry	dry
27.3b	IlvH (A36E)	Pfl01_4787	dry	27.2	DcgH (Q148P)	M	dry	mucoid
5.7a	IlvH (S149R)	Pfl01_4787	dry	5.6a	SadC (25L 4→3)	M	dry	mucoid
5.9e	IlvH (G150S)	Pfl01_4787	dry	5.8b	YfiN (I212T)	M	dry	mucoid
5.10b	IlvI (Δ17bp)	Pfl01_4788	mucoid	5.9b	WspB::D	D	mucoid	dry
5.10a	IlvI (Δ 23bp)	Pfl01_4788	mucoid	5.9b	WspB::D	D	mucoid	dry
6.5a	DgcY (Δ3505-3506)	Pfl01_3505-3506	dry	6.4	WspE (+1bp)	M	dry	mucoid
6.6a	DgcY (Δ3500-3510)	Pfl01_3500-3510	mucoid	6.5a	DgcY (Δ3505-3506)	D	mucoid	dry
2.3	NarA (A383S)	Pfl01_3147	dry	2.2	WspD (W90L)	M	dry	mucoid
10.2	CalM (+5bp)	Pfl01_1895	mucoid	10.1	DgcH (Δ467-470)	D	mucoid	dry
11.2	RndA (Q51S)	Pfl01_2749	mucoid	11.1	WspA (A381V)	D	mucoid	dry
6.8a	CdrB (A290T)	Pfl01_0652	mucoid	6.7c	YfiN (G157C)	D	mucoid	dry

759 ǂ Ancestors are the prototype M or D strains (Fig. 1).

760 * Each mutation was reconstructed in the direct parent and the corresponding ancestor strain. WGS

761 confirmed the reconstruction of each mutation.

762 **Supplementary Information**

Figure S1

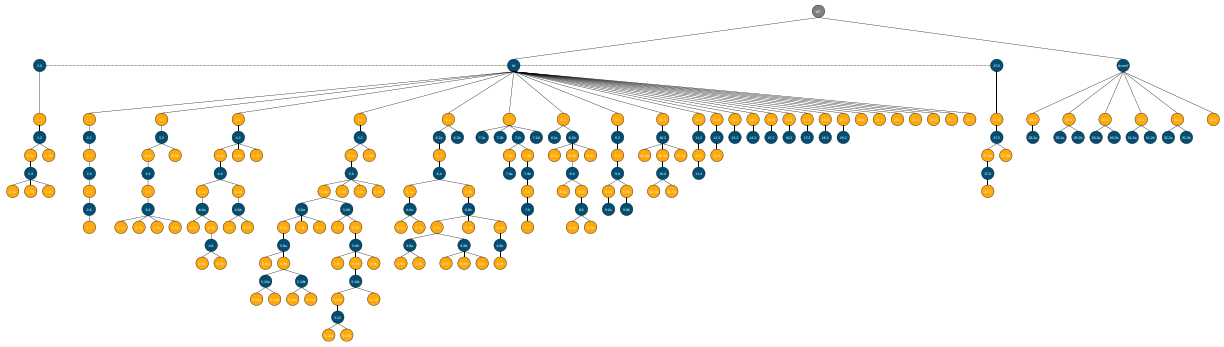

763

764 **Figure S1. Phylogeny of 191 evolved strains across 33 lineages.** Each strain is classified as either D

765 (orange) or M (blue) based on their colony morphology. Corresponding motility data, mutation data,

766 and LC-MS/MS c-di-GMP quantification data are summarized in Table S1.

Figure S2

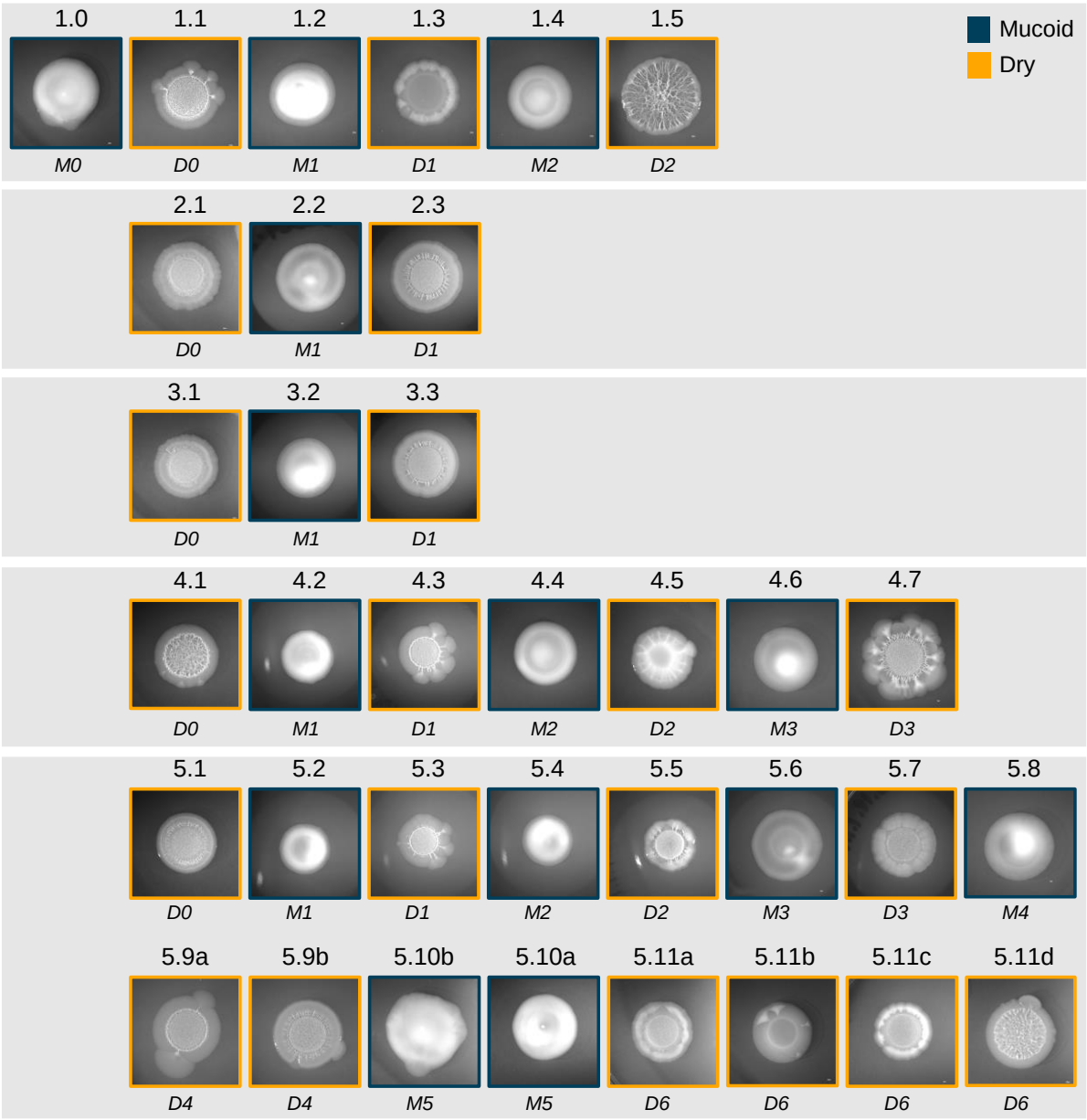

Figure S2. Colony morphologies of evolved strains depicted in Fig. 1B. Each evolved strain is classified either as M (blue) or D (orange) based on their mucoid or dry-wrinkly colony phenotypes, respectively. Motility data and LC-MS/MS c-di-GMP quantification data for each strain are reported in Table S1.

Figure S3

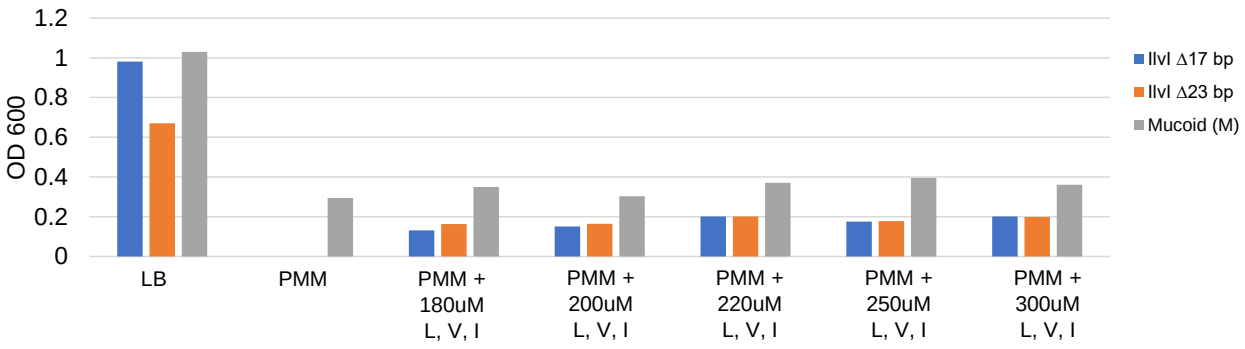

Figure S3. *ilvI* mutants require exogenous supplementation of BCAA. The ancestral M and independently isolated *ilvI* mutant strains were grown in LB (nutrient-rich medium) or PMM (minimal medium) with or without exogenous BCAA supplementation. Both *ilvI* mutants fail to grow in PMM unless supplied with BCAA (leucine (L), valine (V), and isoleucine (I)), and M does not show substantial change in growth with BCAA supplementation.

Table S1. 191 strains isolated from the parallel evolution experiment categorized by lineage.

Strain ID §	Generation §§	Motility Assay †	LC-MS/MS (nM/OD 600) ‡			Locus ***	CDS ID ***	Mutation Location (NT) ***	Consequence ***	Genotype (AA) ***	Genotype (NT) ***
			Replicate A	Replicate B	Replicate C						
WT #	WT	motile	59.23	73.16	62.21	na	na	na	na	na	na
M *	M0	motile	49.19	51.54	48.64	RsmE	Pfl01_1912 ←	2186046	Frame shift	Frame shift	Δ1 bp 126/195 nt
D **	D0	non-motile	187.52	146.52	156.37	WspC	Pfl01_1054 →	1222594	In-frame readthrough	In-frame readthrough	Δ2 bp 1269-1270/1278 nt
1.0 **	M0	motile	49.64	58.15	53.51	WspC	Pfl01_1054 →	1221330	In-frame Δ	Δ*wspC*	Δ5-1278/1278 nt
1.1	D0	non-motile	80.66	94.75	112.01	WspA	Pfl01_1052 →	1220312	Missense	A381V	GCC→GTC
1.2	M1	motile	52.28	59.70	47.26	WspB	Pfl01_1053 →	1221196	Missense	L135P	CTG→CCG
1.3a	D1	non-motile	63.54	81.09	71.31	WspE	Pfl01_1056 →	1225308	In-frame Δ	Δ674-696	Δ2029-2097/2295 nt
1.3b	D1	non-motile				WspE	Pfl01_1056 →	1225307	Duplication	673GMD 1→2	+9bp 2028/2295 nt
1.4	M2	motile	56.99	49.71	49.42	WspE	Pfl01_1056 →	1224117	Frame shift	289*	+1bp 838/2295
1.5a	D2	non-motile	290.55	328.67	307.72	DgcH	Pfl01_0050 ←	55870	Missense	V459G	GTC→GGC
1.5b	D2	non-motile				DgcH	Pfl01_0050 ←	55317	Duplication	+472-643 @ 643	+513bp 1929/2091 nt
1.5c	D2	non-motile				Pfl01_3026	Pfl01_3026 →	3463653	Missense	T242I	ACC→ATC
2.1	D0	non-motile	167.26	267.13	209.38	WspA	Pfl01_1052 →	1220020	In-frame Δ	Δ283-310	Δ850-933/1623 nt
2.2	M1	motile	47.27	41.65	36.89	WspD	Pfl01_1055 →	1222868	Missense	W90L	TGG→TTG
2.3	D1	non-motile	77.37	81.28	110.54	NarA	Pfl01_3147 →	3613968	Missense	A383S	GCC→TCC
2.4	M2	motile				WspD	Pfl01_1055 →	1223197	Nonsense	R200*	CGA→TGA
2.5	D2	non-motile				GcbC	Pfl01_4665 →/ → Pfl01_4666	5266677	5' UTR	+ Pfl01_2031-2032	+1316 +54/-56
2.6	M3	motile				WspA	Pfl01_1052 →	1219276	Nonsense	E36*	GAA→TAA
2.7	D3	non-motile				DgcH	Pfl01_0050 ←	55909	In-frame Δ	Δ441-446	Δ15bp 1323-1337/2091 nt
3.1	D0	non-motile	349.34	359.63	363.90	WspA	Pfl01_1052 →	1220059	In-frame Δ	Δ297-310	Δ889-930/1623 nt
3.2	M1	motile	49.45	51.62	51.41	WspA	Pfl01_1052 →	1220330	Missense	L387R	CTG→CGG
3.3a	D1	non-motile	127.36	112.64	160.92	WspE	Pfl01_1056 →	1225081	Missense	G601V	GGC→GTC
3.3b	D1	non-motile				WspE	Pfl01_1056 →	1224300	Missense	E341K	GAA→AAA
3.4	M2	motile				WspR	Pfl01_1058 →	1227186	Missense	L186Q	CTG→CAG
3.5	D2	non-motile				YfiN	Pfl01_0692 →	818804	Missense	G157A	GGT→GCT
3.6	M3	motile				YfiN	Pfl01_0692 →	819473	In-frame Δ	Δ381-385	Δ1139-1153/1269 nt
3.7a	D3	non-motile				DgcX	Pfl01_3550 →	4023270	Missense	M350I	ATG→ATA
3.7b	D3	non-motile				GcbC	Pfl01_4665 →/ → Pfl01_4666	5266677	5' UTR	+ Pfl01_2031-2032	+1316 +54/-56
3.7c	D3	non-motile				MorA	Pfl01_4876 →	5499015	Missense	M991I	ATG→ATA
3.7d	D3	non-motile				MorA	Pfl01_4876 →	5499101	Missense	A1020E	GCG→GAG
4.1	D0	non-motile	145.66	170.85	148.76	DgcH	Pfl01_0050 ←	55647	In-frame Δ	Δ524-537	Δ1558-1599/2091 nt
4.2	M1	motile	42.78	46.36	47.13	DgcH	Pfl01_0050 ←	55345	Missense	L634P	CTC→CCC
4.3a	D1	non-motile	392.53	328.69	404.68	WspA	Pfl01_1052 →	1220309	Missense	V380A	GTC→GCC
4.3b	D1	non-motile				WspF	Pfl01_1057 →	1226046	Missense	S159L	TCG→TTG
4.3c	D1	non-motile				WspA	Pfl01_1052 →	1220170	In-frame Δ	Δ334-336	Δ1000-1008/1623 nt
4.4	M2	motile	50.14	53.49	61.31	WspE	Pfl01_1056 →	1224447	Missense	D390N	GAC→AAC
4.5a	D2	non-motile	81.95	81.25	75.76	WspA	Pfl01_1052 →	1220020	In-frame Δ	Δ283-310	Δ850-933/1623 nt
4.5b	D2	non-motile				WspA	Pfl01_1052 →	1219961	Missense	Q264L	CAG→CTG
4.6a	M3	motile	57.50	54.72	51.88	WspE	Pfl01_1056 →	1224601	Missense	V441A	GTG→GCG
4.6b	M3	motile	54.52	56.68	55.08	WspD	Pfl01_1055 →	1223058	In-frame Δ	Δ152-157	Δ459-476/684 nt
4.7a	D3	non-motile	275.45	268.03	177.32	WspE	Pfl01_1056 →	1224693	Missense	S472C	AGT→TGT
4.7b	D3	non-motile				GcbC	Pfl01_4665 →/ → Pfl01_4666	5266677	5' UTR	+ Pfl01_2031-2032	+1316 +54/-56
4.7c	D3	non-motile				FleN	Pfl01_1562 →	1752356	Missense	T13I	ACC→ATC
4.7d	D3	non-motile				CysH	Pfl01_1757 ←	1952544	Nonsense	W51*	TGG→TGA
4.8	M4	motile				GcbC	Pfl01_4666 →	5268046	Frame shift	Frame shift	+1bp 1314/1506 nt
4.9a	D4	non-motile				DgcY	Pfl01_3502	3982758	Frame shift	Frame shift	Δ502-555/672 nt
4.9b	D4	non-motile				MorA	Pfl01_4876 →	5498817	Missense	M925I	ATG→ATC
5.1	D0	non-motile	106.41	95.85	119.21	WspF	Pfl01_1057 →	1225883	Missense	P105S	CCG→TCG
5.2	M1	motile	39.11	39.97	57.53	WspA	Pfl01_1052 →	1220156	In-frame Δ	Δ329	Δ986-988/1623 nt
5.3a	D1	non-motile	158.40	145.92	166.92	WspA	Pfl01_1052 →	1220017	In-frame Δ	Δ283-296	Δ847-888/1623 nt
5.3b	D1	non-motile				WspA	Pfl01_1052 →	1220020	In-frame Δ	Δ283-310	Δ850-933/1623 nt
5.4	M2	motile	40.20	67.63	44.65	WspD	Pfl01_1055 →	1223058	In-frame Δ	Δ152-157	Δ459-476/684 nt
5.5a	D2	non-motile	131.86	92.83	93.92	SadC	Pfl01_4451 ←	5013023	5' UTR	5' UTR	A→T (-11)
5.5b	D2	non-motile				SadC	Pfl01_4451 ←	5013023	5' UTR	5' UTR	A→C (-11)
5.5c	D2	non-motile				SadC	Pfl01_4451 ←	5013023	5' UTR	5' UTR	A→C (-11)
5.5d	D2	non-motile				WspE	Pfl01_1056 →	1224211	Duplication	308RMV 1→2	+9bp 932/2295
5.6a	M3	motile	49.79	50.94	43.86	SadC	Pfl01_4451 ←	5012937	In-frame Δ	25L 4→3	Δ74-76/1107 nt
5.6b	M3	motile				SadC	Pfl01_4451 ←	5012937	In-frame Δ	25L 4→3	Δ74-76/1107 nt
5.7a	D3	non-motile	68.79	59.84	78.79	IlvH	Pfl01_4787 ←	5402643	Missense	S149R	AGT→AGG
5.7b	D3	non-motile				DgcH	Pfl01_0050 ←	55647	In-frame Δ	Δ524-537	Δ1558-1599/2091 nt
5.7c	D3	non-motile				WspE	Pfl01_1056 →	1225351	Missense	D691G	GAC→GGC
5.7d	D3	non-motile				WspE	Pfl01_1056 →	1224324	Missense	R349S	CGC→AGC
5.7e	D3	non-motile				YfiN	Pfl01_0692 →	818804	Missense	G157A	GGT→GCT
5.8a	M4	motile	54.44	51.70	73.94	ParA	Pfl01_0730 →	858438	Missense	D115N	GAT→AAT

5.8b	M4	motile	47.61	37.67	40.41	YfiN	Pfl01_0692 →	818969	Missense	I212T	ATT→ACT
5.9a	D4	non-motile	329.69	230.96	263.57	WspA	Pfl01_1052 →	1220649	In-frame Δ	wspA::D	Δ2421 bp
5.9b	D4	non-motile	92.77	95.21	136.41	WspB	Pfl01_1053 →	1220923	In-frame Δ	wspB::D	Δ1840 bp
5.9c	D4	non-motile				WspE	Pfl01_1056 →	1223451	Missense	R58W	CGG→TGG
5.9d	D4	non-motile				WspE	Pfl01_1056 →	1223648	Missense	M123I	ATG→ATA
5.9e	D4	non-motile	53.36	63.66	60.18	IlvH	Pfl01_4787 ←	5402642	Missense	G150S	GGC→AGC
5.10a	M5	motile	56.96	56.62	55.12	IlvI	Pfl01_4788 ←	5403629	Frame shift	Frame shift	Δ23bp 1166-1188/1725 nt
5.10b	M5	motile	49.96	49.89	107.61	IlvI	Pfl01_4788 ←	5403629	Frame shift	Frame shift	Δ17bp 1172-1188/1725 nt
5.10c	M5	motile				WspR	Pfl01_1058 →	1227150	Missense	T174I	ACC→ATC
5.11a	D5	non-motile	110.47	109.78	180.81	WspE	Pfl01_1056 →	1223648	Missense	M123I	ATG→ATA
5.11b	D5	non-motile	104.23	129.78	152.89	WspE	Pfl01_1056 →	1225239	In-frame Δ	Δ653-656	Δ12bp 1960-1971/2295 nt
5.11c	D5	non-motile	81.07	77.14	96.70	WspE	Pfl01_1056 →	1224144	Missense	D289N	GAC→AAC
5.11d	D5	non-motile	128.07	115.76	132.55	DgcH	Pfl01_0050 ←	55647	In-frame Δ	Δ524-537	Δ1558-1599/2091 nt
5.11e	D5	non-motile				GcbC	Pfl01_4665 →/ → Pfl01_4666	5266677	5' UTR	+ Pfl01_2031-2032	+1316 +54/-56
5.11f	D5	non-motile				MorA	Pfl01_4876 →	5499284	Missense	E1081A	GAA→GCA
5.12	M6	motile				GcbC	Pfl01_4666 →	5266862	Missense	A44P	GCC→CCC
5.13a	D6	non-motile				MorA	Pfl01_4876 →	5499088	In-frame Δ	Δ1015-1020	Δ15bp 3046-3060/3849 nt
5.13b	D6	non-motile				GcbC	Pfl01_4666 →	5267723	Missense	A331T	GCC→ACC
6.1	D0	non-motile				WspF	Pfl01_1057 →	1226544	Frame shift	KI325R*	Δ974/1011 nt
6.2a	M1	motile				WspA	Pfl01_1052 →	1219239	Duplication	L23 2→3	+3bp 69/1623
6.2b	M1	motile				WspR	Pfl01_1058 →	1227374	Missense	G249C	GGC→TGC
6.3	D1	non-motile				WspA	Pfl01_1052 →	1219239	Duplication	L24 3→2	-3bp 69/1623
6.4	M2	motile	51.19	81.77	61.87	WspE	Pfl01_1056 →	1225435	Frame shift	748*	+1bp 2156/2295 nt
6.5a	D2	non-motile	189.04	141.94	135.43	DgcY	[Pfl01_3505]–Pfl01_3506	3985701	In-frame Δ	124* Δ5' UTR 3508	Δ3505,Δ3506,Δ3508 5'UTR
6.5b	D2	non-motile				SadC	Pfl01_4451 ←	5013023	5' UTR	5' UTR	A→C (-11)
6.6a	M3	motile	69.41	59.49	94.44	DgcY	[Pfl01_3500]–Pfl01_3510	3981080	In-frame Δ	Δ10 proteins	Δ3500-3510
6.6b	M3	motile				SadC	Pfl01_4451 ←	5012937	In-frame Δ	25L 4→3	Δ74-76/1107 nt
6.7a	D3	non-motile				CheB	Pfl01_1567	1758645	Frame shift	Frame shift	Δ1bp 1061/1137 nt
6.7b	D3	non-motile				FlgF	Pfl01_1501 →	1680303	Frame shift	Frame shift	Δ14bp 138-151/741 nt
6.7c	D3	non-motile	66.67	50.69	60.25	YfiN	Pfl01_0692 →	818803	Missense	G157C	GGT→TGT
6.7d	D3	non-motile				DgcH	Pfl01_0050 ←	55952	Frame shift	Δ430	Δ1292-1294/2091 nt
6.7e	D3	non-motile				YfiR	Pfl01_0691 →	817876	In-frame Δ	Δ37-61	Δ114-188/576 nt
6.8a	M4	motile	41.34	42.22	39.91	CdrB	Pfl01_0652 ←	763630	Missense	A290T	GCC→ACC
6.8b	M4	motile				YfiN	Pfl01_0692 →	819458	Missense	A375V	GCG→GTG
6.8c	M4	motile				YfiN	Pfl01_0692 →	818709	Frame shift	Frame shift	+1bp 375/1269 nt
6.9a	D4	non-motile				DgcH	Pfl01_0050 ←	55978	Missense	L423P	CTC→CCC
6.9b	D4	non-motile				MorA	Pfl01_4876 →	5499015	Missense	M991I	ATG→ATA
6.9c	D4	non-motile				MorA	Pfl01_4876 →	5499015	Missense	M991I	ATG→ATT
6.9d	D4	non-motile				DgcH	Pfl01_0050 ←	55647	In-frame Δ	Δ524-537	Δ1558-1599/2091 nt
6.9e	D4	non-motile				GcbC	Pfl01_4665 →/ → Pfl01_4666	5266677	5' UTR	+ Pfl01_2031-2032	+1316 +54/-56
6.9f	D4	non-motile				RapA	Pfl01_1678 ←	1873535	Missense	S317A	TCG→GCG
7.1	D0	non-motile	187.52	146.52	156.37	WspC	Pfl01_1054 →	1222594	In-frame Δ	*wspC::D*	Δ1269-1270/1278 nt
7.2a	M1	motile				WspE	Pfl01_1056 →	1223360	Frame shift	156*	+1bp 81/2295 nt
7.2b	M1	motile				WspR	Pfl01_1058 →	1227186	Frame shift	205*	Δ1bp 557/1002 nt
7.2c	M1	motile				WspD	Pfl01_1055 →	1223058	In-frame Δ	Δ152-157	Δ459-476/684 nt
7.2d	M1	motile				WspD	Pfl01_1055 →	1223058	In-frame Δ	Δ152-157	Δ459-476/684 nt
7.3a	D1	non-motile				WspE	Pfl01_1056 →	1223648	Missense	M123I	ATG→ATA
7.3b	D1	non-motile				WspE	Pfl01_1056 →	1224162	Missense	R295C	CGC→TGC
7.4a	M2	motile				WspD	Pfl01_1055 →	1222912	Nonsense	Q105*	CAG→TAG
7.4b	M2	motile				WspE	Pfl01_1056 →	1224637	Missense	H453R	CAC→CGC
7.5	D2	non-motile				SadC	Pfl01_4451 ←	5013023	5' UTR	5' UTR	A→C (-11)
7.6	M3	motile				SadC	Pfl01_4451 ←	5012937	In-frame Δ	25L 4→3	Δ74-76/1107 nt
7.7	D3	non-motile				MorA	Pfl01_4876 →	5498240	Missense	S733L	TCG→TTG
8.1	D0	non-motile				WspF	Pfl01_1057 →	1226036	Missense	I156R	ATC→CGA
8.2a	M1	motile				WspC	Pfl01_1054 →	1222439	Nonsense	Q372*	CAG→TAG
8.2b	M1	motile				WspD	Pfl01_1055 →	1223283	Missense	*228C (WspD::E)	TGA→TGC
8.3a	D1	non-motile				GcbC	Pfl01_4665 →/ → Pfl01_4666	5266677	5' UTR	+ Pfl01_2031-2032	+1316 +54/-56
8.3b	D1	non-motile				MorA	Pfl01_4876 →	5499015	Missense	M991I	ATG→ATA
8.3c	D1	non-motile				MorA	Pfl01_4876 →	5499286	Missense	E1082K	GAA→AAA
8.4	M2	motile				MorA	Pfl01_4876 →	5497033	Frame shift	487*	+4bp 991/3849nt
8.5a	D2	non-motile				DgcH	Pfl01_0050 ←	55773	In-frame Δ	Δ413-491	Δ1237-1473/2091 nt
8.5b	D2	non-motile				DgcX	Pfl01_3550 →	4023270	Missense	M350I	ATG→ATA
8.6	M3	motile				DgcX	Pfl01_3550 →	4023085	In-frame Δ	Δ289	Δ3bp 865-867/1680 nt
8.7a	D3	non-motile				YfiN	Pfl01_0692 →	818891	Missense	P186R	CCG→CGG
8.7b	D3	non-motile				FliI	Pfl01_1539 →	1729003	Frame shift	Frame shift	+1bp 1015/1359 nt
9.1	D0	non-motile				WspF	Pfl01_1057 →	1226393	Missense	G275W	GGG→TGG
9.2	M1	motile				WspE	Pfl01_1056 →	1223361	Frame shift	38*	Δ82-127/2295 nt
9.3	D1	non-motile				YfiN	Pfl01_0692 →	818803	Missense	G157S	GGT→AGT

9.4	M2	motile				YfiN	Pfl01_0692 →	819523	Nonsense	Q397*	CAA→TAA
9.5a	D2	non-motile				DgcH	Pfl01_0050 ←	55896	In-frame Δ	Δ445-450	Δ1333-1350/2091 nt
9.5b	D2	non-motile				DgcH	Pfl01_0050 ←	55647	In-frame Δ	Δ524-537	Δ1558-1599/2091 nt
9.6a	M3	motile				tRNA	Pfl01_R0084 ←	5451395	5' UTR	5' UTR	G→T 49/77nt
9.6b	M3	motile				RplV	Pfl01_5074 ←	5702436	Missense	A43T	GCC→ACC
10.1	D0	non-motile	301.71	271.29	205.50	DgcH	Pfl01_0050 ←	55835	In-frame Δ	Δ467-470	Δ1400-1411/2091 nt
10.2	M1	motile	48.63	48.06	46.64	CalM	Pfl01_1895 →	2166348	Frame shift	Frame shift	+5bp 1685/2652 nt
10.3a	D1	non-motile				CalM	Pfl01_1895 →	2166348	In-frame Δ	In-frame Δ	-5bp 1685/2652 nt
10.3b	D1	non-motile				WspF	Pfl01_1057 →	1226204	Nonsense	E212*	GAA→TAA
10.3c	D1	non-motile				CalM	Pfl01_1895 →	2166348	In-frame Δ	In-frame Δ	-5bp 1685/2652 nt
10.4	M2	motile				WspR	Pfl01_1058 →	1226823	Missense	L65Q	CTG→CAG
10.5	D2	non-motile				CalM	Pfl01_1895 →	2166348	In-frame Δ	In-frame Δ	-5bp 1685/2652 nt
11.1	D0	non-motile	80.66	94.75	112.01	WspA	Pfl01_1052 →	1220312	Missense	A381V	GCC→GTC
11.2	M1	motile	49.17	51.38	65.08	RndA	Pfl01_2749 ←	3170622	Nonsense	Q51*	CAG→TAG
11.3	D1	non-motile	147.33	132.67	152.43	DgcH	Pfl01_0050 ←	55647	In-frame Δ	Δ524-537	Δ1558-1599/2091 nt
11.4	M2	motile	43.58	37.94	43.96	WspR	Pfl01_1058 →	1226967	Missense	A113D	GCC→GAC
12.1	D0	non-motile				WspE	Pfl01_1056 →	1225222	Missense	D648G	GAC→GGC
12.2	M1	motile				WspC	Pfl01_1054 →	1222526	Frame shift	421*	Δ1201-1202/1278 nt
12.3	D1	non-motile				WspA	Pfl01_1052 →	1220020	In-frame Δ	Δ283-310	Δ850-933/1623 nt
13.1	D0	non-motile				WspF	Pfl01_1057 →	1225581	Missense	A4E	GCA→GAA
13.2	M1	motile				WspC	Pfl01_1054 →	1222479	Missense	H385P	CAC→CCC
14.1	D0	non-motile				WspF	Pfl01_1057 →	1226127	Missense	H186P	CAT→CCT
14.2	M1	motile				WspA	Pfl01_1052 →	1220333	Missense	S388F	TCC→TTC
15.1	D0	non-motile				WspE	Pfl01_1056 →	1225307	Duplication	673GMD 1→2	+9bp 2028/2295 nt
15.2	M1	motile				WspF	Pfl01_1057 →	1226474	Missense	S302R	AGT→CGT
16.1	D0	non-motile				WspF	Pfl01_1057 →	1225883	Missense	P105S	CCG→TCG
16.2	M1	motile				WspC	Pfl01_1054 →	1221551	Nonsense	E76*	GAA→TAA
17.1	D0	non-motile				WspF	Pfl01_1057 →	1226391	Missense	T274I	ACA→ATA
17.2	M1	motile				WspA	Pfl01_1052 →	1219453	Nonsense	Q95*	CAG→TAG
18.1	D0	non-motile				WspF	Pfl01_1057 →	1225721	In-frame Δ	Δ48-52	Δ151-165/1011 nt
18.2	M1	motile				WspR	Pfl01_1058 →	1226688	Nonsense	L20*	TTG→TAG
19.1	D0	non-motile				WspA	Pfl01_1052 →	1220020	In-frame Δ	Δ283-310	Δ850-933/1623 nt
19.2	M1	motile				WspE	Pfl01_1056 →	1223907	Frame shift	Frame shift	-1 bp 628/2295
20	D0	non-motile				WspF	Pfl01_1057 →	1226559	Nonsense	L330*	TTG→TAG
21	D0	non-motile				WspF	Pfl01_1057 →	1225721	In-frame Δ	Δ48-52	Δ151-165/1011 nt
22	D0	non-motile				WspA	Pfl01_1052 →	1220020	In-frame Δ	Δ283-310	Δ850-933/1623 nt
23	D0	non-motile				WspF	Pfl01_1057 →	1225883	Missense	P105S	CCG→TCG
24	D0	non-motile				MorA	Pfl01_4876 →	5499286	Missense	E1082K	GAA→AAA
25	D0	non-motile				WspE	Pfl01_1056 →	1224324	Missense	R349S	CGC→AGC
26	D0	non-motile				MorA	Pfl01_4876 →	5498817	Missense	M925I	ATG→ATA
27.0 **	M0	motile				WspC	Pfl01_1054 →	1221330	In-frame Δ	Δ*wspCD*	Δ1954/1954 nt
27.1	D0	non-motile				DgcH	Pfl01_0050 ←	55873	Missense	Q458P	CAG→CCG
27.2	M1	motile	42.70	39.96	36.29	DgcH	Pfl01_0050 ←	56803	Missense	Q148P	CAG→CCG
27.3a	D1	non-motile	47.26	71.96	72.99	IlvH	Pfl01_4787 ←	5402983	Missense	A36E	GCG→GAG
27.3b	D1	non-motile				FlgL	Pfl01_1507 ←	1687852	Frame shift	326*	Δ1bp 866/1572 nt
27.4	M2	motile				WspB	Pfl01_1053 →	1221329	Missense	*179C (WspB+)	TGA→TGC
27.5	D2	non-motile				MorA	Pfl01_4876 →	5498222	Missense	V727A	GTA→GCA
ΔrsmE *	M0	motile	61.11	61.63	60.13	RsmE	Pfl01_1912 ←	2185977	In-frame Δ	Δ*rsmE*	Δ1-195/195 nt
28.1	D0	non-motile				WspA	Pfl01_1052 →	1220020	In-frame Δ	Δ283-310	Δ850-933/1623 nt
28.2	M1	motile				WspA	Pfl01_1052 →	1220716	Nonsense	Q516*	CAG→TAG
29.1	D0	non-motile				WspE	Pfl01_1056 →	1225506	Missense	K743Q	AAG→CAG
29.2a	M1	motile				WspC	Pfl01_1054 →	1221416	Frame shift	51*	+ 19bp 91/1278 nt
29.2b	M1	motile				WspA	Pfl01_1052 →	1219453	Nonsense	Q95*	CAG→TAG
30.1	D0	non-motile				WspF	Pfl01_1057 →	1226123	Nonsense	Q185*	CAG→TAG
30.2a	M1	motile				WspR	Pfl01_1058 →	1227012	Frame shift	138*	Δ1bp 383/1002 nt
30.2b	M1	motile				WspC	Pfl01_1054 →	1222448	Frame shift	389*	Δ1bp 1123/1278 nt
31.1	D0	non-motile				WspC	Pfl01_1054 →	1222342	In-frame Δ	WspC::D	Δ305bp WspC:WspD
31.2a	M1	motile				WspA	Pfl01_1052 →	1220714	Missense	R515P	CGT→CCT
31.2b	M1	motile				WspA	Pfl01_1052 →	1220099	Missense	T310N	ACC→AAC
32.1	D0	non-motile				WspE	Pfl01_1056 →	1225223	Missense	D648G	GAC→GAA
32.2a	M1	motile				WspA	Pfl01_1052 →	1219957	Missense	S263P	TCC→CCC
32.2b	M1	motile				WspB	Pfl01_1053 →	1221235	Nonsense	W148*	TGG→TAG
33.1	D0	non-motile	86.13	60.82	85.85	WspF	Pfl01_1057 →	1225721	In-frame Δ	Δ48-52	Δ151-165/1011 nt

778 § Relationships of the lineages presented here are visualized in Fig. S1. Strain IDs correspond to variant calling files found in 'Table S1 - Source Data 1' that

779 provides evidence for each reported mutation. All strains were generated in this experiment unless otherwise noted or stated here: *[62]; ** [24]; # [52]. M and

780 D served as the prototype ancestral strains throughout this study.

781 §§ Generation refers to an individual strain's evolutionary distance from WT where the following sequence represents the accumulation of mutations at each

782 generation: WT, M0, D0, M1, D1, … M6, D6.

783 † Determined by stab-motility assays.

784 ‡ Select strains were chosen for LC-MS/MS c-di-GMP quantification conducted in triplicate.

785 *** Locus, CDS, and Mutation Location (NT) were extracted from GenBank reference CP000094 unless otherwise stated. CDS: → (+ strand), ← (- strand), /

786 (intergenic space). Genotype (AA/NT) was reported by BreSeq during variant analysis. Consequence describes the nature of mutation.

Table S2. Node-edge plot data matrix.

Source	Target	Attribute	Count
CdrB	DgcH	D	1
CdrB	MorA	D	1
ParA	WspA	D	1
ParA	WspB	D	1
CalM	CalM	D	2
CalM	WspF	D	1
RndA	DgcH	D	1
NarA	WspD	M	1
DgcY	Pfl01_1567	D	1
DgcY	FlgF	D	1
DgcY	DgcY	M	1
DgcX	Pfl01_1539	D	1
DgcX	YfiN	D	1
DgcX	DgcX	M	1
SadC	DgcH	D	2
SadC	IlvH	D	1
SadC	MorA	D	1
SadC	WspE	D	2
SadC	YfiN	D	2
SadC	YfiR	D	1
SadC	SadC	M	4
DgcH	FlgL	D	1
DgcH	IlvH	D	1
DgcH	WspA	D	2
DgcH	WspF	D	1
DgcH	CalM	M	1
DgcH	DgcH	M	2
DgcH	R0084	M	1
DgcH	RplV	M	1
DgcH	WspR	M	1
GcbC	DgcY	D	1
GcbC	GcbC	D	1
GcbC	MorA	D	2
GcbC	GcbC	M	1
IlvH	ParA	M	1
IlvH	WspB	M	1
IlvI	DgcH	D	1
IlvI	WspE	D	3
MorA	DgcX	D	1
MorA	DgcH	D	1
MorA	MorA	M	1
RsmE	DgcH	D	2
RsmE	WspA	D	4
RsmE	WspD	D	1
RsmE	WspE	D	2
RsmE	WspF	D	15
RsmE	WspD	M	1
WspA	NarA	D	1
WspA	DgcH	D	1
WspA	WspA	D	3
WspA	WspE	D	2
WspA	RndA	M	1
WspA	WspA	M	4
WspA	WspB	M	1
WspA	WspD	M	3
WspA	WspE	M	5
WspB	MorA	D	1
WspB	WspE	D	2
WspB	IlvI	M	2
WspC	DgcH	D	1
WspC	WspA	D	2
WspC	WspE	D	1
WspC	WspD	M	2
WspC	WspE	M	1
WspC	WspR	M	1
WspD	Pfl01_1562	D	1
WspD	Pfl01_1757	D	1
WspD	SadC	D	3
WspD	GcbC	D	2
WspD	MorA	D	2
WspD	WspA	D	1
WspD	WspD	D	1
WspD	WspE	D	3
WspD	WspA	M	3
WspE	Pfl01_3026	D	1
WspE	DgcY	D	1
WspE	SadC	D	2
WspE	DgcH	D	2
WspE	GcbC	D	1
WspE	MorA	D	2
WspE	WspA	D	2
WspE	WspE	D	1
WspE	YfiN	D	1
WspE	WspA	M	2
WspE	WspB	M	1
WspE	WspC	M	2
WspE	WspE	M	2
WspE	WspR	M	2
WspF	WspA	M	4
WspF	WspC	M	4
WspF	WspD	M	1
WspF	WspE	M	2
WspF	WspR	M	4
WspR	CalM	D	2
WspR	GcbC	D	1
WspR	MorA	D	1
WspR	YfiN	D	1
YfiN	DgcX	D	1
YfiN	DgcH	D	3
YfiN	GcbC	D	2
YfiN	IlvH	D	1
YfiN	MorA	D	3
YfiN	RapA	D	1
YfiN	WspE	D	2
YfiN	CdrB	M	1
YfiN	YfiN	M	4
YfiR	YfiN	M	1

* Values are reported in to-from format with source indicating the mutation a parent strain carries, target indicating the mutation a daughter cell carries, attribute indicating if said daughter cell's mutation resulted in the M or D phenotype, and count indicating the frequency of the pattern in the dataset.

792 **Table S3. Description of PCR primers used to reconstruct mutations.**

Target mutation	Forward Primer Sequence	Reverse Primer Sequence
WspA::D	ATCTGGTGAACGCCAAACT	TGACCAGGCAATCTTCCATC
WspB::D	CCACGTATGACATCGAACAGA	CTGTCGAGATCGAGCAGTTC
WspC::D	TGCCGAGAACGAAGGTTA	CTGTCGAGATCGAGCAGTTC
IlvH (A36E)	CAAGACGGAGCGTACCTAATC	AACGGTAGCCGAACCTTTAC
IlvH (S149R)	CAAGACGGAGCGTACCTAATC	AACGGTAGCCGAACCTTTAC
IlvH (G150S)	CAAGACGGAGCGTACCTAATC	AACGGTAGCCGAACCTTTAC
IlvI (Δ17bp)	AGGGAAGCTCAAAGCGATAC	AACCTGCCGGTTACCAATAC
IlvI (Δ 23bp)	AGGGAAGCTCAAAGCGATAC	AACCTGCCGGTTACCAATAC
DgcY (Δ3505-3506)	ATGGCTAAGCCCAGTTACACA	TGAAGCCGTTGAGATCGATA
DgcY (Δ3500-3510)	ATCGTTAGGGCGCTATCAATAC	TTGCATCGAGCAGGGTTTTC
NarA (A383S)	CATTTACACCTCGGGAGATGAC	CGACAGCGCATTGAAGAAAC
CalM (+5bp)	CTGCTGACCAATCCAATCCT	AAGTCATCGTCTGCCAACTC
RndA (Q51S)	TTGTTCACTCATCGCCTACTG	CGACCAGCGTTCCGATAAA
CdrB (A290T)	CGTTATCAACAGGACGGCTATC	GCTTGAGTTCCAGACCGTTATT
ilvH external check	CGCACTCCTACATGGAATCA	CAGCTACATCGGTCACTTTCA
ilvI external check	AAGCCAAACTGCGTTCCTA	TTCATCTGGATACTGCCTTCAC

793

794

795

796 **Table S1 – Source Data 1. BreSeq summary reports of mutations identified in strains isolated in this**

797 **study.** Whole genome sequencing data of select strains from the parallel evolution experiments were

798 subjected to variant analysis using the BreSeq algorithm against the published *P. fluorescens* Pf0-1

799 genome sequence. Summary files are provided for each analysis where the 'Strain ID' reported in Table

800 S1 is represented as the file name.

801

802 **Acknowledgments**

803 We thank RTSF (Michigan State University) for services and assistance with LC-MS/MS analyses and

804 MiGS (Pittsburgh, PA) for providing genome sequencing. This study was funded by the Charles Henry

805 Leach II Fund (W.K.) and the Faculty Development Fund (W.K.) awarded by Duquesne University.

806

807 **Author Contributions**

808 W.K. designed the study, C.K. performed the experiments, C.K and W.K analyzed data and wrote the

809 manuscript.

810

811 **Conflict of Interest**

812 The authors declare no conflict of interest.

813

814 **References**

815 1. Römling U, Galperin MY, Gomelsky M. Cyclic di-GMP: the First 25 Years of a Universal Bacterial
816 Second Messenger. Microbiology and Molecular Biology Reviews. 2013;77: 1–52.
817 doi:10.1128/MMBR.00043-12
818 2. Valentini M, Filloux A. Biofilms and Cyclic di-GMP (c-di-GMP) Signaling: Lessons from
819 Pseudomonas aeruginosa and Other Bacteria. Journal of Biological Chemistry. 2016;291: 12547–
820 12555. doi:10.1074/jbc.R115.711507
821 3. Wolfe AJ, Visick KL. Get the message out: Cyclic-Di-GMP regulates multiple levels of flagellum-
822 based motility. Journal of Bacteriology. 2008. doi:10.1128/JB.01418-07
823 4. Jenal U, Reinders A, Lori C. Cyclic di-GMP: second messenger extraordinaire. Nature Reviews
824 Microbiology. 2017;15: 271–284. doi:10.1038/nrmicro.2016.190
825 5. Tamayo R. Cyclic diguanylate riboswitches control bacterial pathogenesis mechanisms. PLoS
826 Pathogens. 2019;15. doi:10.1371/journal.ppat.1007529
827 6. Dahlstrom KM, Giglio KM, Sondermann H, O'Toolea GA. The inhibitory site of a diguanylate
828 cyclase is a necessary element for interaction and signaling with an effector protein. Journal of
829 Bacteriology. 2016;198: 1595–1603. doi:10.1128/JB.00090-16
830 7. Simm R, Morr M, Kader A, Nimtz M, Römling U. GGDEF and EAL domains inversely regulate cyclic
831 di-GMP levels and transition from sessility to motility. Molecular Microbiology. 2004;53: 1123–
832 1134. doi:10.1111/j.1365-2958.2004.04206.x
833 8. Hengge R, Galperin MY, Ghigo JM, Gomelsky M, Green J, Hughes KT, et al. Systematic
834 nomenclature for GGDEF and EAL domaincontaining cyclic di-GMP turnover proteins of
835 Escherichia coli. Journal of Bacteriology. 2016;198: 7–11. doi:10.1128/JB.00424-15
836 9. Newell PD, Yoshioka S, Hvorecny KL, Monds RD, O'Toole GA. Systematic Analysis of Diguanylate
837 Cyclases That Promote Biofilm Formation by *Pseudomonas fluorescens* Pf0-1. Journal of
838 Bacteriology. 2011;193: 4685–4698. doi:10.1128/JB.05483-11
839 10. Huertas-Rosales Ó, Romero M, Heeb S, Espinosa-Urgel M, Cámara M, Ramos-González MI. The
840 Pseudomonas putida CsrA/RsmA homologues negatively affect c-di-GMP pools and biofilm
841 formation through the GGDEF/EAL response regulator CfcR. Environmental Microbiology.
842 2017;19: 3551–3566. doi:10.1111/1462-2920.13848

843 11. Merritt JH, Ha D-G, Cowles KN, Lu W, Morales DK, Rabinowitz J, et al. Specific Control of
844 Pseudomonas aeruginosa Surface-Associated Behaviors by Two c-di-GMP Diguanylate Cyclases.
845 Newman DK, editor. mBio. 2010;1. doi:10.1128/mBio.00183-10
846 12. Ravichandran A, Ramachandran M, Suriyanarayanan T, Wong CC, Swarup S. Global Regulator
847 MorA Affects Virulence-Associated Protease Secretion in Pseudomonas aeruginosa PAO1. PLOS
848 ONE. 2015;10: e0123805. doi:10.1371/journal.pone.0123805
849 13. Wassmann P, Chan C, Paul R, Beck A, Heerklotz H, Jenal U, et al. Structure of BeF3--Modified
850 Response Regulator PleD: Implications for Diguanylate Cyclase Activation, Catalysis, and
851 Feedback Inhibition. Structure. 2007. doi:10.1016/j.str.2007.06.016
852 14. Moscoso JA, Jaeger T, Valentini M, Hui K, Jenal U, Filloux A. The diguanylate cyclase SadC is a
853 central player in Gac/Rsm-mediated biofilm formation in Pseudomonas aeruginosa. Journal of
854 Bacteriology. 2014;196: 4081–4088. doi:10.1128/JB.01850-14
855 15. Giardina G, Paiardini A, Fernicola S, Franceschini S, Rinaldo S, Stelitano V, et al. Investigating the
856 allosteric regulation of YfiN from Pseudomonas aeruginosa: Clues from the structure of the
857 catalytic domain. PLoS ONE. 2013;8. doi:10.1371/journal.pone.0081324
858 16. De N, Pirruccello M, Krasteva PV, Bae N, Raghavan RV, Sondermann H. Phosphorylation-
859 Independent Regulation of the Diguanylate Cyclase WspR. Lory S, editor. PLoS Biology. 2008;6:
860 e67. doi:10.1371/journal.pbio.0060067
861 17. Kessler C, Mhatre E, Cooper V, Kim W. Evolutionary divergence of the Wsp signal transduction
862 system in β- And γ-proteobacteria. Appl Environ Microbiol. 2021;87.
863 doi:10.1101/2021.07.02.450980
864 18. Mantoni F, Paiardini A, Brunotti P, D'Angelo C, Cervoni L, Paone A, et al. Insights into the GTP-
865 dependent allosteric control of c-di-GMP hydrolysis from the crystal structure of PA0575 protein
866 from Pseudomonas aeruginosa. FEBS Journal. 2018;285. doi:10.1111/febs.14634
867 19. Giacalone D, Smith TJ, Collins AJ, Sondermann H, Koziol LJ, O'Toole GA. Ligand-mediated biofilm
868 formation via enhanced physical interaction between a diguanylate cyclase and its receptor.
869 mBio. 2018;9. doi:10.1128/mBio.01254-18
870 20. Christen B, Christen M, Paul R, Schmid F, Folcher M, Jenoe P, et al. Allosteric Control of Cyclic di-
871 GMP Signaling. Journal of Biological Chemistry. 2006;281: 32015–32024.
872 doi:10.1074/jbc.M603589200
873 21. Chan C, Paul R, Samoray D, Amiot N, Giese B, Jenal U, et al. Structural basis for the activity and
874 allosteric control of diguanylate cyclase. Acta Crystallographica Section A Foundations of
875 Crystallography. 2005. doi:10.1107/s0108767305089993
876 22. De N, Navarro MVAS, Raghavan R v., Sondermann H. Determinants for the Activation and
877 Autoinhibition of the Diguanylate Cyclase Response Regulator WspR. Journal of Molecular
878 Biology. 2009;393: 619–633. doi:10.1016/j.jmb.2009.08.030
879 23. Dahlstrom KM, Collins AJ, Doing G, Taroni JN, Gauvin TJ, Greene CS, et al. A multimodal strategy
880 used by a large c-di-GMP network. Journal of Bacteriology. 2018;200. doi:10.1128/JB.00703-17
881 24. Kim W, Levy SB, Foster KR. Rapid radiation in bacteria leads to a division of labour. Nature
882 Communications. 2016;7: 10508. doi:10.1038/ncomms10508
883 25. Spiers AJ, Kahn SG, Bohannon J, Travisano M, Rainey PB. Adaptive divergence in experimental
884 populations of *Pseudomonas fluorescens*. I. Genetic and phenotypic bases of wrinkly spreader
885 fitness. Genetics. 2002;161: 33–46.

886 26. Bantinaki E, Kassen R, Knight CG, Robinson Z, Spiers AJ, Rainey PB. Adaptive Divergence in
887 Experimental Populations of *Pseudomonas fluorescens*. III. Mutational Origins of Wrinkly
888 Spreader Diversity. Genetics. 2007;176: 441–453. doi:10.1534/genetics.106.069906
889 27. Armbruster CR, Lee CK, Parker-Gilham J, de Anda J, Xia A, Zhao K, et al. Heterogeneity in surface
890 sensing suggests a division of labor in *Pseudomonas aeruginosa* populations. Elife. 2019;8: 1–29.
891 doi:10.7554/eLife.45084
892 28. O'neal L, Baraquet C, Suo Z, Dreifus JE, Peng Y, Raivio TL, et al. The Wsp system of Pseudomonas
893 aeruginosa links surface sensing and cell envelope stress. 2022. doi:10.1073/pnas
894 29. Re S da, Tolstykh T, Wolanin PM, Stock JB. Genetic analysis of response regulator activation in
895 bacterial chemotaxis suggests an intermolecular mechanism. Protein Science. 2002;11: 2644–
896 2654. doi:10.1110/ps.0220402
897 30. Bellsolell L, Prieto J, Serrano L, Coll M. Magnesium Binding to the Bacterial Chemotaxis Protein
898 CheY Results in Large Conformational Changes Involving its Functional Surface. Journal of
899 Molecular Biology. 1994;238: 489–495. doi:10.1006/jmbi.1994.1308
900 31. Huangyutitham V, Güvener ZT, Harwood CS. Subcellular Clustering of the Phosphorylated WspR
901 Response Regulator Protein Stimulates Its Diguanylate Cyclase Activity. Kolter R, editor. mBio.
902 2013;4: 1–8. doi:10.1128/mBio.00242-13
903 32. Wei Q, Leclercq S, Bhasme P, Xu A, Zhu B, Zhang Y, et al. Diguanylate cyclases and
904 phosphodiesterases required for basal-level c-di-GMP in Pseudomonas aeruginosa as revealed by
905 systematic phylogenetic and transcriptomic analyses. Applied and Environmental Microbiology.
906 2019;85. doi:10.1128/AEM.01194-19
907 33. Rice MS, Dahlquist FW. Sites of deamidation and methylation in Tsr, a bacterial chemotaxis
908 sensory transducer. Journal of Biological Chemistry. 1991;266: 9746–9753. doi:10.1016/S0021-
909 9258(18)92884-X
910 34. Levit MN, Stock JB. Receptor methylation controls the magnitude of stimulus-response coupling
911 in bacterial chemotaxis. Journal of Biological Chemistry. 2002;277. doi:10.1074/jbc.M204325200
912 35. Li Y, Hu Y, Fu W, Xia B, Jin C. Solution structure of the bacterial chemotaxis adaptor protein CheW
913 from Escherichia coli. Biochemical and Biophysical Research Communications. 2007;360.
914 doi:10.1016/j.bbrc.2007.06.146
915 36. Chauhan JS, Mishra NK, Raghava GPS. Identification of ATP binding residues of a protein from its
916 primary sequence. BMC Bioinformatics. 2009;10. doi:10.1186/1471-2105-10-434
917 37. Fang X, Ahmad I, Blanka A, Schottkowski M, Cimdins A, Galperin MY, et al. GIL, a new c-di-GMP-
918 binding protein domain involved in regulation of cellulose synthesis in enterobacteria. Molecular
919 Microbiology. 2014;93. doi:10.1111/mmi.12672
920 38. Carman GM, Han GS. Roles of phosphatidate phosphatase enzymes in lipid metabolism. Trends in
921 Biochemical Sciences. 2006. doi:10.1016/j.tibs.2006.10.003
922 39. Ricca E, Limauro D, Lago CT, de Felice M. Enhanced acetohydroxy acid synthase III activity in an
923 ilvH mutant of Escherichia coli K-12. J Bacteriol. 1988;170. doi:10.1128/jb.170.11.5197-
924 5199.1988
925 40. Massie JP, Reynolds EL, Koestler BJ, Cong J-P, Agostoni M, Waters CM. Quantification of high-
926 specificity cyclic diguanylate signaling. Proceedings of the National Academy of Sciences.
927 2012;109: 12746–12751. doi:10.1073/pnas.1115663109

928 41. Yan J, Deforet M, Boyle KE, Rahman R, Liang R, Okegbe C, et al. Bow-tie signaling in c-di-GMP:
929 Machine learning in a simple biochemical network. Igoshin OA, editor. PLOS Computational
930 Biology. 2017;13: e1005677. doi:10.1371/journal.pcbi.1005677
931 42. Shannon P, Markiel A, Ozier O, Baliga NS, Wang JT, Ramage D, et al. Cytoscape: A software
932 Environment for integrated models of biomolecular interaction networks. Genome Research.
933 2003;13. doi:10.1101/gr.1239303
934 43. Petelski AN, Fonseca Guerra C. Designing Self-Assembled Rosettes: Why Ammeline is a Superior
935 Building Block to Melamine. ChemistryOpen. 2019;8. doi:10.1002/open.201800210
936 44. Reichhardt C, Wong C, da Silva DP, Wozniak DJ, Parsek MR. CDRA interactions within the
937 pseudomonas aeruginosa biofilm matrix safeguard it from proteolysis and promote cellular
938 packing. mBio. 2018;9. doi:10.1128/mBio.01376-18
939 45. Cooley RB, Smith TJ, Leung W, Tierney V, Borlee BR, O'Toole GA, et al. Cyclic di-GMP-regulated
940 periplasmic proteolysis of a Pseudomonas aeruginosa type Vb secretion system substrate.
941 Journal of Bacteriology. 2016;198: 66–76. doi:10.1128/JB.00369-15
942 46. Borlee BR, Goldman AD, Murakami K, Samudrala R, Wozniak DJ, Parsek MR. *Pseudomonas*
943 *aeruginosa* uses a cyclic-di-GMP-regulated adhesin to reinforce the biofilm extracellular matrix.
944 Molecular Microbiology. 2010;75: 827–842. doi:10.1111/j.1365-2958.2009.06991.x
945 47. Wehbi H, Portillo E, Harvey H, Shimkoff AE, Scheurwater EM, Howell PL, et al. The peptidoglycan-
946 binding protein fimv promotes assembly of the pseudomonas aeruginosa type IV pilus secretin.
947 Journal of Bacteriology. 2011;193. doi:10.1128/JB.01048-10
948 48. Buendia L, Girardin A, Wang T, Cottret L, Lefebvre B. LysM receptor-like kinase and lysM
949 receptor-like protein families: An update on phylogeny and functional characterization. Frontiers
950 in Plant Science. 2018. doi:10.3389/fpls.2018.01531
951 49. Conner JG, Zamorano-Sánchez D, Park JH, Sondermann H, Yildiz FH. The ins and outs of cyclic di-
952 GMP signaling in Vibrio cholerae. Current Opinion in Microbiology. 2017;36: 20–29.
953 doi:10.1016/j.mib.2017.01.002
954 50. Soto SM. Role of efflux pumps in the antibiotic resistance of bacteria embedded in a biofilm.
955 Virulence. 2013;4. doi:10.4161/viru.23724
956 51. Liang F, Zhang B, Yang Q, Zhang Y, Zheng D, Zhang L, et al. Cyclic-di-GMP Regulates the Quorum-
957 Sensing System and Biocontrol Activity of Pseudomonas fluorescens 2P24 through the RsmA and
958 RsmE Proteins. Applied and Environmental Microbiology. 2020;86. doi:10.1128/aem.02016-20
959 52. Compeau G, Al-Achi BJ, Platsouka E, Levy SB. Survival of rifampin-resistant mutants of
960 Pseudomonas fluorescens and Pseudomonas putida in soil systems. Applied and Environmental
961 Microbiology. 1988;54. doi:10.1128/aem.54.10.2432-2438.1988
962 53. Kirner S, Krauss S, Sury G, Lam ST, Ligon JM, van Pée KH. The non-haem chloroperoxidase from
963 Pseudomonas fluorescens and its relationship to pyrrolnitrin biosynthesis. Microbiology (N Y).
964 1996;142. doi:10.1099/13500872-142-8-2129
965 54. Matthews M, Roy CR. Identification and subcellular localization of the Legionella pneumophila
966 IcmX protein: A factor essential for establishment of a replicative organelle in eukaryotic host
967 cells. Infection and Immunity. 2000;68. doi:10.1128/IAI.68.7.3971-3982.2000
968 55. Winsor GL, Griffiths EJ, Lo R, Dhillon BK, Shay JA, Brinkman FSL. Enhanced annotations and
969 features for comparing thousands of *Pseudomonas* genomes in the Pseudomonas genome
970 database. Nucleic Acids Research. 2016;44: D646–D653. doi:10.1093/nar/gkv1227

971 56. Lu S, Wang J, Chitsaz F, Derbyshire MK, Geer RC, Gonzales NR, et al. CDD/SPARCLE: the conserved
972 domain database in 2020. Nucleic Acids Research. 2020;48: D265–D268. doi:10.1093/nar/gkz991
973 57. Kim W, Levy SB. Increased fitness of Pseudomonas fluorescens Pf0-1 leucine auxotrophs in soil.
974 Applied and Environmental Microbiology. 2008;74: 3644–3651. doi:10.1128/AEM.00429-08
975 58. Feng X, Lilly AA, Hazelbauer GL. Enhanced Function Conferred on Low-Abundance
976 Chemoreceptor Trg by a Methyltransferase-Docking Site. Journal of Bacteriology. 1999;181:
977 3164–3171. doi:10.1128/JB.181.10.3164-3171.1999
978 59. Alexander RP, Lowenthal AC, Harshey RM, Ottemann KM. CheV: CheW-like coupling proteins at
979 the core of the chemotaxis signaling network. Trends in Microbiology. 2010;18: 494–503.
980 doi:10.1016/j.tim.2010.07.004
981 60. Malone JG, Williams R, Christen M, Jenal U, Spiers AJ, Rainey PB. The structure–function
982 relationship of WspR, a *Pseudomonas fluorescens* response regulator with a GGDEF output
983 domain. Microbiology (N Y). 2007;153: 980–994. doi:10.1099/mic.0.2006/002824-0
984 61. O'Connor JR, Kuwada NJ, Huangyutitham V, Wiggins PA, Harwood CS. Surface sensing and lateral
985 subcellular localization of WspA, the receptor in a chemosensory-like system leading to c-di-GMP
986 production. Mol Microbiol. 2012;86: 720–9. doi:10.1111/mmi.12013
987 62. Kim W, Racimo F, Schluter J, Levy SB, Foster KR. Importance of positioning for microbial
988 evolution. Proceedings of the National Academy of Sciences. 2014;111: E1639–E1647.
989 doi:10.1073/pnas.1323632111
990